Understanding composite negative differential resistance in niobium oxide memristors

Xinjun Liu,[1, a)] Peng Zhang,[1] Shimul Kanti Nath,[2] Shuai Li,[3] Sanjoy Kumar Nandi,[2] and Robert Glen Elliman[2]

[1]*Tianjin Key Laboratory of Low Dimensional Materials Physics and Preparation Technology, Faculty of Science, Tianjin University, Tianjin 300354, People's Republic of China*

[2]*Department of Electronic Materials Engineering, Research School of Physics and Engineering, The Australian National University, Canberra ACT 2601, Australia*

[3]*Unité Mixte de Physique CNRS/Thales, Université Paris-Saclay, 91767 Palaiseau, France*

Volatile memristor, also called as threshold switching, exhibits an S-type negative differential resistance (S-NDR) phenomenon on the current–voltage curve. Studying the origin of NDR is of great significance for exploring the potential applications in nano-oscillators and neuromorphic computing. Here, we provide a reasonable explanation of the physical origin of multiple complex NDR phenomena in niobium oxide. First, a core memristor–shell resistor model is constructed by considering the fact that there is a conductive filament in the oxide device. When the shell resistance R_S is a linear resistance, the critical resistance R_C and the maximum absolute NDR value R_{NDR} are recognized as the dividing lines to determine three shapes of current–voltage curves; when the R_S is a nonlinear resistance, the basic S-NDR curve and Snap-back NDR (SB-NDR) curve observed in experiments are qualitatively reproduced. Then, based on the assumption of multi-filaments and infinite R_S, a dual-core memristor model is constructed to achieve a series of complex multi-NDR coexistence curves, including dual S-NDR and combined S-SB NDR. These simulation results were analysed in detail that the current distribution is not uniform and has complex spatio-temporal behavior when current is flowing through the oxide device. Finally, the device with double S-NDR phenomenon is put into the oscillation circuit to observe the oscillation behavior. The oscillation appears, disappears, then reappears and finally re-disappears as the total voltage V_T increases with the fixed load resistance R_L. Two oscillation regions are plotted on the V_T–R_L diagram, which is qualitatively consistent with the double-window oscillation behavior observed in the experiments. This discovery further illustrates that the multiple types of NDR phenomena have many unproven potential applications.

Keywords: Memristor, Negative differential resistance, Volatile memristor, Core–shell model

a) Electronic mail: xinjun.liu@tju.edu.cn

I. INTRODUCTION

The current-controlled negative differential resistance (CC-NDR) phenomenon has great potential in the construction of circuit components and has been widely used in electronic circuits. Related functional devices include threshold switch, signal amplifier, comparator, high-frequency oscillator, chaotic oscillator, etc.[1] Recently, the CC-NDR phenomenon also shows the application prospects in emerging technologies. For example, the neuron spikes generated by the CC-NDR device can be used to implement neuromorphic calculation, which helps to build neural networks and realize brain-like computing.[2,3] The CC-NDR phenomenon can usually be observed in transition oxides NbO_x, VO_2, TaO_x and TiO_x.[4-6] The devices made of these oxides have the advantages of simple preparation, miniaturization, low cost, and compatibility with semiconductor processes, etc, which bring great prospects for the study of artificial neural networks and their neuromorphic calculations. However, researchers have disputes on the basic physical mechanism of CC-NDR,[5,7-10] especially for the composite NDR reported recently.[2,11-17] Therefore, ascertaining the physical origin of CC-NDR is very important for practical applications.

In order to obtain the electrical characteristics of microelectronic devices, there are usually two measurement modes to record the current–voltage (*I*–*V*) curve. One is to apply a series of voltages to the device and then measure the current passing through it, that is, **the voltage-sweeping (VS) mode**; another is to apply a series of currents to the device and then measure the voltage thereon, that is, **the current-sweeping (CS) mode**. For linear electronic devices, the *I*–*V* curves obtained by the two modes are consistent. However, for nonlinear electronic devices, the *I*–*V* curves obtained by the two modes are not necessarily the same. For example, in a CC-NDR device, the *I*–*V* curve obtained in the CS mode is a smooth S-type NDR (S-NDR) curve (Fig. **1(a)**), while in the VS mode the device current discontinuously jumps near the threshold voltage (Fig. **1(c)**), resulting in a *I*–*V* curve with hysteresis region. The S-NDR or hysteresis threshold switching phenomenon of the device is generally considered to be related to thermal runaway caused by thermal feedback, but its fundamental physical mechanism is still controversial. In 2018, Gibson[10] proposed that any two-port device, as long as its conductance and temperature are super-linearly dependent, can generate a thermally driven S-NDR phenomenon. He verified this view theoretically by using five different conduction mechanisms.

However, in the actual research of S-NDR device, it is found that the *I*–*V* curves obtained in the CS mode are not always smooth S-NDR curves. There are often some small discontinuous voltage 'steps',[8] and sometimes even large discontinuities snap-back NDR (SB-NDR) phenomenon, as shown in Fig. **1(b)**.[14] It differs from S-NDR in that single current value corresponds to multiple voltage values and the high resistance state and the low resistance state are discontinuous. In 1968, Stanford et al[18] observed a highly nonlinear discontinuous SB-NDR behavior with hysteresis in amorphous chalcogenide materials. This discovery led many research groups to try to understand the generation mechanism of SB-NDR. The SB-NDR characteristic also exists in oxide materials such as VO_x,[19,20] TaO_x,[16,21,22] and NbO_x.[2,14] The reasons for the SB-NDR characteristics are still very controversial. In 2019, Goodwill et al.[16] also observed SB-NDR behaviors in TaO_x-based threshold switching devices. They observed the spontaneous current contraction phenomenon by using a scanning Joule heating electron microscope (SJEM), which provided an explanation for SB-NDR behavior. In 2019, Nandi et al.[14] observed stable SB-NDR in the Nb/NbO_x/Pt devices by controlling the experimental conditions, such as changing the thickness of NbO_x, oxygen content, and device size, etc. They used in-situ thermal reflection imaging to observe the dynamic change of the temperature distribution on the surface of the device, and conclude that the snapback response is caused by the localization and redistribution of current in the oxide film. It should be noted that when VS mode is performed on the same Nb/NbO_x/Pt device, the threshold switch hysteresis curve is also observed, as shown in Fig. **1(d)**. In other words, the VS mode cannot distinguish between S-NDR and SB-NDR curves. Therefore, in order to clearly understand the *I*–*V* characteristics of the NbO_x thin film, it is necessary to measure it with CS mode.

The two S-NDR and SB-NDR curves mentioned above are the simplest and most typical basic NDR curves. These two NDRs can coexist in the same device in many ways, forming a series of complex composite NDR phenomena. A typical example is that in 2017, Kumar et al.[2] in HP Lab observed the coexistence of the S-NDR and the SB-NDR in the nano-scale niobium oxide memristor using the CS mode. They used thermo-reflectance to measure the device temperature during switching and show that the S-NDR occurred at ~390 K while the SB-NDR occurred at ~1000 K. Based on these observations it was concluded that the smooth, low-temperature S-NDR was consistent with Poole–Frenkel (P–F) conduction while the high-temperature SB-NDR was consistent with the Mott insulator–metal transition (IMT) in NbO_2. In 2019, Herzig et al.[17] also observed a complex NDR phenomenon in the NDR region based on NbO_x threshold switching devices, which they called the multi-slope NDR phenomenon, and attributed this result to instrumental measurements. In 2019, Li et al.[13] observed experimentally not only three types of *I*–*V* curves mentioned above, but also other types of *I*–*V* curves, including double S-NDR, double SB-NDR and multi-cross-type NDR phenomena. Starting from the generalized power exponent relationship between conductance and temperature, combined with Newton's law of cooling, they reproduced the single S-NDR phenomenon driven by heat, and used the core–shell memristor model to conduct hybrid NDR and other NDR phenomena.

In this work, we exploit two core–shell models and analyse various NDR phenomena in the *I*–*V* curves. Based on the uneven distribution of current in the NbO_x film, the reason for the discontinuous hysteresis SB-NDR curve and the generation details of various coexistence NDR characteristics are obtained. Finally, by studying the double S-NDR devices, it can realize the function of double window oscillation in the oscillation circuit, which is consistent with the preliminary experimental results.

II. CORE MEMRISTOR–SHELL RESISTANCE STRUCTURE MODEL

To realize the threshold switching function for transition metal oxides such as NbO_x, VO_2, TaO_x, TiO_2, etc.,[23-25] it is necessary to be subjected to a critical electroforming process to form local conductive filaments. Bohaichuk et al.[26] and Nath et al.[27] applied a layer of light-sensitive organic substances on the surface of VO_2 and NbO_x devices, respectively. After applying a large voltage, a soft breakdown phenomenon occurred. The presence of conductive filaments was directly observed with an optical microscope, and the positioning of the conductive filaments was achieved. The threshold switching function of the device is realized by Joule heating. The I–V characteristics of device are closely related to the microscopic material composition and current density redistribution. It is reasonable for research to assume the NbO_x device as a **core memristor–shell resistor (cM–sR)** structure.

Figure **2(a)** shows a schematic diagram of the **cM–sR** structure, in which the inner red cylindrical region represents the core memristor R_M, and the outer yellow region wrapped represents the shell resistance R_S. R_M is equivalent to the local conductive filament formed in the device after electroforming process, and R_S is equivalent to the region around the conductive filament. When performing CS mode on the device, the current will pass through the two regions of R_M and R_S, respectively. Their current depends on the relative conductivity of the core and shell films and the temperature distribution in the device. It is defined that I_T is the total current of the current source, V_T is the total voltage. I_M and I_S are the currents through the R_M and R_S, respectively. V_M and V_S are the voltages on the R_M and R_S, respectively.

It is generally considered that the R_M with a higher temperature is the functional area that produces the S-NDR phenomenon, and the R_S with a colder temperature acts as a large resistance. For simplification, we ignore the thermal exchange between the two areas, then the **cM–sR** structure can be simplified to the parallel structure shown in Fig **2(b)**, namely R_M and large resistance R_S in parallel. When conducting a CS mode of this device, the current mainly passes through the core region, and the current through the shell region is generally negligible. The obtained I_T–V_T curve is approximately the inherent I–V curve of the core memristor, that is, the S-NDR curve. In the following study, we will gradually reduce the constant R_S, then increase the I_S, and observe the changing characteristics of the I_M–V_M curve and synthetic I_T–V_T curve.

2.1 LINEAR SHELL RESISTANCE

Using the P–F conduction mechanism and Newton's law of cooling (see Equation **S1** and **S2** in the supplementary material), the NDR characteristics of the core memristor are constructed to study the combined I_T–V_T characteristics of different **cM–sR** parallel structure models. Figure **3(a)** shows the inherent *I*–*V* curve of the core memristor, with typical S-NDR behavior. The *I*–*V* curve of threshold switching has two characteristic points, namely the threshold point (V_{th} = 1.547 V, I_{th} = 78.5 μA) and the hold point (V_h = 0.963 V, I_h = 2.36 mA). Through these two characteristic points, the critical resistance $R_C = \frac{V_{th}-V_h}{I_h-I_{th}}$ is defined, and its value is about 256 Ω. Figure **3(b)** shows the relationship between the differential resistance $\frac{dV}{dI}$ and the current *I*. The $\frac{dV}{dI}$ has a negative maximum value in the NDR region, as point **A** marked in Fig. **3(b).** The absolute value of the maximum $\frac{dV}{dI}$ is defined as $R_{NDR} = \left|\frac{dV}{dI}\right|_{max}$, and its value is about 1167 Ω. It can also be seen from Fig. **3(b)** that, except for point **A**, the arbitrarily determined $\frac{dV}{dI}$ in the NDR region corresponds to two points on the $\frac{dV}{dI} - I$ curve, that is, the same $\frac{dV}{dI}$ has two corresponding current values.

2.1.1 I_M–V_M characteristics of core memristor

The parallel connection between S-NDR and constant resistance is the simplest combination in the **cM–sR** model. By combining the *I*–*V* curve of S-NDR core and the linear *I*–*V* curve, a synthetic I_T–V_T curve will be obtained. In parallel state under test, the I_M–V_M curve of the S-NDR core memristor and the I_S–V_S curve of shell resistance are different from those in their individual state. When a CS mode is applied to the equivalent circuit of the **cM–sR** model, the state equations of this circuit can be listed by Kirchhoff's law:

$$I_T = I_M + I_S = \frac{V_M}{R_M} + \frac{V_S}{R_S} \tag{1}$$

$$V_T = V_M = V_S \tag{2}$$

It can be obtained through transformation:

$$I_T = V_M\left(\frac{1}{R_M} + \frac{1}{R_S}\right) = V_M\left(\frac{R_M+R_S}{R_M R_S}\right) \tag{3}$$

The voltage V_M and current I_M on the S-NDR device are further derived as:

$$V_M = I_T\left(\frac{R_M R_S}{R_M+R_S}\right) \tag{4}$$

$$I_M = \frac{V_M}{R_M} = I_T\left(\frac{R_M R_S}{R_M+R_S}\right)\cdot\frac{1}{R_M} = \frac{I_T R_S}{R_M+R_S} \tag{5}$$

From Equations (4) and (5), the differential resistance $\frac{dV_M}{dI_M}$ on the S-NDR device is obtained:

$$\frac{dI_M}{dV_M} = \left(\frac{dI_M}{dR_M}\right) / \left(\frac{dV_M}{dR_M}\right) = \left(-\frac{I_T R_S}{(R_M+R_S)^2}\right) / \left(\frac{I_T R_S^2}{(R_M+R_S)^2}\right) = -\frac{1}{R_S} \quad (6)$$

$$\frac{dV_M}{dI_M} = \left(\frac{dV_M}{dR_M}\right) / \left(\frac{dI_M}{dR_M}\right) = \left(\frac{I_T R_S^2}{(R_M+R_S)^2}\right) / \left(-\frac{I_T R_S}{(R_M+R_S)^2}\right) = -R_S \quad (7)$$

It can be seen from Equation (7) that the $\frac{dV_M}{dI_M}$ value in the NDR region is exactly equal to the negative shell resistance. Based on this, the I_M–V_M curve of the S-NDR core memristor in parallel state can be drawn on the basis of I–V curve in Fig. 3(a). Take R_S = 500 Ω as an example, as shown in Fig. 3(c), the specific process is as follows:

(1) According to Equation (7), the $\frac{dV_M}{dI_M}$= –500 Ω, which corresponds to points B and C in Fig. 3(b). The current values of these two points are 83.6 μA and 0.998 mA, respectively.

(2) Redraw the S-NDR curve in Fig. 3(a), and mark the two points B and C corresponding to these two current values on the S-NDR curve in Fig. 3(c).

(3) Starting from points B and C, make straight lines with a slope of $-\frac{1}{R_S}$, and they intersect the S-NDR curve at the higher current point B' (0.991 V, 1.48 mA) and the lower current point C' (1.382 V, 0.31 mA).

(4) After removing the line segment (indicated by the black dashed line) located in the B–B'–C–C' area, it is the I_M–V_M curve on the core memristor after 500 Ω shell resistance is connected in parallel.

In the same way, we can draw the I_M–V_M curve on the core memristor after 180 Ω of R_S is connected in parallel, as shown in Fig. 3(d). The area of D–D'–E–E' region is larger than the area of B–B'–C–C' region. Obviously, there is no hysteresis area of I_M–V_M curve when R_S > R_{NDR}, while the hysteresis area of I_M–V_M curve gradually increases as R_S decreases when R_S < R_{NDR}. In addition, B' is right below the hold point while D' (0.979 V, 3.25 mA) is right above the hold point. It infers that the R_C is also a critical value. These are consistent with the I_M–V_M results obtained in the following simulation.

2.1.2 Adjusting shell linear resistance

Shukla et al.[28] connected a load resistor R_L with different resistance values in series with VO_2 device and found two types of hysteresis and non-hysteresis I_M–V_M curves by performing VS mode. They calculated the critical resistance R_C that produced these two curves. Slesazeck et al.[29] used R_{NDR} as the dividing line for the stability of the entire local active region on the I–V characteristic in the case of VS mode and the R_L connected in series with the NbO_2 device. Gibson[10] believes that a non-hysteresis

NDR region is observed on the device when $R_S > R_{NDR}$, and the I_M–V_M curve on the device exists hysteresis area when $R_S < R_{NDR}$. All these works are based on the application of VS mode on the basis of series resistance R_L, while our work is based on the application of CS mode on the basis of parallel resistance R_S. In according to whether there are characteristic hysteresis regions on the I_T–V_T curve and where the hysteresis regions appear, the three typical I_T–V_T curves have been observed. In the simulation, by continuously changing the value of R_S, three typical I_T–V_T curve correspond to the three ranges of $R_S > R_{NDR}$, $R_C < R_S < R_{NDR}$, and $R_S < R_C$.

Here, the $R_C \approx 256\ \Omega$ and $R_{NDR} = 1167\ \Omega$ of the core memristor. The red straight line in Fig. **4(a)–(c)** gives the *I*–*V* characteristics of three specific cases, $R_S = 1200\ \Omega$, $R_S = 400\ \Omega$, and $R_S = 180\ \Omega$, and different slopes represent different degrees of linearity. The black curves in Fig. **4(a)–(c)** give the *I*–*V* characteristics of the same core memristor. Put the R_M and the R_S in parallel into the circuit, that is, the combination of the red straight line and the black curve, and the blue combined I_T–V_T curve in Fig. **4(d)–(f)** will be obtained.

When the shell resistance is 1200 Ω, $R_S > R_{NDR}$, no hysteresis region is observed, the circuit state is in a stable circuit state. that is, typical S-NDR phenomenon (Fig. **4(d)**). When the shell resistance is 400 Ω and 180 Ω, $R_S < R_{NDR}$, there is a hysteresis region in the combined I_T–V_T curve, as shown in Figs **4(e)** and **4(f)**. The circuit state is in an unstable circuit state, both of them produce lateral voltage jumps, that is, the SB-NDR phenomenon. Careful observation shows that when the R_S is 400 Ω, the point P (0.991 V, 3.96 mA) to which the voltage jump returns appears in the NDR area. The P is located below the hold point ($V_h = 0.963$ V, $I_h = 4.77$ mA), we defined this type NDR as the SB1-NDR phenomenon. When the shell resistance is 180 Ω, the point Q to which the voltage jump returns appears in the positive resistance area. The Q (0.979 V, 8.69 mA) is located above the hold point ($V_h = 0.963$ V, $I_h = 7.71$ mA), we defined this type NDR as the SB2-NDR phenomenon. Obviously, the hysteresis area of SB2-NDR is larger than that of SB1-NDR. This has been confirmed in the experiments (see Fig. **S1** in the supplementary material). The composite I_T–V_T curve in the high resistance region is approximately equal to *I*–*V* of the parallel R_S in three cases, while the composite I_T–V_T curve in the low resistance state meets the superposition of dynamic resistances. Considering the shunt effect of the R_S, there are difference between the I_T–V_T curve and the I_M–V_M curve on the device. Fig. **4(g)–(i)** show the I_M–V_M and I_S–V_S curves in three cases. The slope of I_M–V_M curve in the NDR region is $-\frac{1}{R_S}$. Although the I_S–V_S curve is still a straight line, the I_S has jump behavior in the I_S–*t* curve.

During the CS mode on the **cM–sR** model, the voltage V_M on the R_M is same with the voltage V_S on the R_S at any time. It is meaningful to compare their resistance under the same voltage. Hence, we performed the VS mode on the R_M and R_S to compare their differential resistances, as shown in Fig. **5(a)**. The R_S is much smaller than the differential resistance $\left(\frac{dV}{dI}\right)_M$ of the R_M in the same voltage (~217 kΩ @ 0.1 V), as shown in Fig. **5(b)**. Hence, the current mainly go through the shell region when the current is applied on the **cM–sR** model. Take R_S = 180 Ω as an example, $I_S > I_M$, as shown in Fig. **5(c)**. In time scale, both the I_M and I_S change suddenly at certain time. The current I_S decrease, while the current I_M increase significantly. The dynamic resistance $\frac{dV_T}{dI_T}$ meets the parallel superposition of dynamic resistances $\frac{dV_M}{dI_M}$ and $\frac{dV_S}{dI_S} = R_S$ at any time (Fig. **5(d)**).

Note that same I_M–V_M curves can also be obtained in the circuit of S-NDR series with load resistance $R_L = R_S$ measuring in VS model (see Fig. **S2** in the supplementary material). Load-line analysis is fit for both cases of parallel R_S with CS mode and series R_L with VS mode (see Fig. **S3** in the supplementary material).

2.2 MONOTONE NONLINEAR SHELL RESISTANCE

In the actual situation, the composite I_T–V_T curve in the high resistance region is a monotone nonlinear state. The current increases nonlinearly with the voltage increasing (see Figs. **1(a)** and **1(b)**), showing a semiconductor-like diode or Schottky-like junction characteristics.[15] Hence, it is reasonable to construct a nonlinear R_S. Shimul et al.[15] have used the Schottky-like conduction mechanism as nonlinear R_S to explain a polarity dependence NDR response of Nb/NbO_x/Pt cross-point devices. In this study, we use P–F conduction mechanism to construct a nonlinear R_S.

Since the shell and the core represent different regions of the same oxide film, it is reasonable to consider that their electrical conductivity is controlled by the same physical mechanism, i.e. P–F conduction mechanism. Considering that the cross-sectional area of the shell layer is much larger than that of the core layer, the thermal effect of the surrounding environment can be ignored. The monotonically reduced nonlinear R_S is directly obtained by removing the Newton's cooling law as shown in below.

When studying the effect of nonlinear R_S on the combined *I*–*V* characteristics of the **cM–sR** model, a series of different nonlinear characteristics were selected for research by only changing the activation energy E_a from 0.22 eV to 0.16 eV in the P–F conductivity model (see Table **S1** in the supplementary material). As shown in the red curves in Fig. **6(a)–(c)**, the three curves have different degrees of curvature in the high-voltage region, representing different degrees of nonlinearity. The black curves in Fig. **6(a)–(c)** give the *I*–*V* characteristics of the same core memristor. To combine the red and black curves, we put the R_M and the non-linear R_S in parallel into the circuit, then obtain the blue combined I_T–V_T curve in Fig. **6(d)–(f)**. The composite I_T–V_T curve in the high resistance region is approximately equal to *I*–*V* characteristics of the parallel R_S. Fig. **6(g)–(i)** show the I_M–V_M and I_S–V_S curves in three cases.

The VS mode on the R_M and R_S was performed to compare their dynamic resistances, as shown in Figs **7(a)**. Since the differential resistance $\left(\frac{dV}{dI}\right)_S$ of the parallel R_S is smaller than the differential resistance $\left(\frac{dV}{dI}\right)_M$ (~217 kΩ @ 0.1 V) of the R_M, as shown in Figs **7(b)**, the current mainly goes through the shell region at the initial low current applied (Fig. **7(c)**). Although the I_S–V_S curve is still smooth in whole region (Fig. **6(i)**), I_S change not continuously in time scale (Fig. **7(c)**). The jump upward of I_M is observed in I_M–*t* curve (Fig. **7(c)**). The composite I_T–V_T curve in the high and low resistance region meets the superposition of dynamic resistances (Fig. **7(d)**).

The combined I_T–V_T curve exhibits nonlinear characteristics in the high-resistance state, which is qualitatively consistent with the actual measured curve (see Figs. **1(a)** and **1(b)**). Similar to the linear R_S, the **cM–sR** combination I_T–V_T curve with nonlinear R_S has three categories of S-NDR, SB1-NDR and SB2-NDR. It is important to understand how the nonlinear R_S affects the NDR behavior. The combined I_T–V_T hysteresis curve in Fig. **6(e)** and **(f)** produces lateral bending of voltage. The points of nonlinear R_S that determine the characteristics of I_T–V_T curve are A, B, C, D, E and F in Fig. **6(a)–(c)**, which are the mapping points of the V_{th} and V_h of the R_M. The corresponding $\frac{dV}{dI}$ values are 1.32 kΩ, 3.58 kΩ, 0.28 kΩ, 0.76 kΩ, 0.13 kΩ, and 0.35 kΩ, as seen in Fig. **7(b)**.

Here, the $R_C \approx 256\ \Omega$ and $R_{NDR} = 1167\ \Omega$ of the core memristor. Since the dynamic resistance value $\left(\frac{dV}{dI}\right)_S$ = 1.32 kΩ > R_{NDR} at A in Fig. **6(a)**, the combined I_T–V_T curve still exhibits S-NDR behavior in Fig. **6(d)**. The dynamic values of R_S at C and E in Fig. **6(b)** and **(c)** are $R_C < \left(\frac{dV}{dI}\right)_S$ =280 Ω < R_{NDR} and $\left(\frac{dV}{dI}\right)_S$ = 130 Ω <R_C, and the synthesized I_T–V_T curve shows hysteresis behavior in Figs. **6(e)** and **6(f)**. Careful observation shows that in Fig. **6(e)**, the point U (0.997 V, 1.95 mA) to which the voltage jump returns appears in the NDR area. The U is located below the hold point (V_h = 0.963 V, I_h = 2.86 mA), this is the SB1-NDR phenomenon. When in Fig. **6(f)**, the point W to which the voltage jump returns appears in the positive resistance area. The W (0.973 V, 4.16 mA) is located above the hold point (V_h = 0.963 V, I_h = 3.47 mA), this is the SB2-NDR phenomenon. Obviously, the hysteresis area of SB2-NDR is larger than that of SB1-NDR. In response to this, some parameters can be controlled in the experiment to adjust the R_S to achieve a specific NDR behavior. These parameters include the area of the device and the oxygen content of the NbO_x layer.[14] When the $\left(\frac{dV}{dI}\right)_S$ value of the R_S is several orders of magnitude lower than the high resistance of the core memristor, the nonlinear R_S determines the combination I_T–V_T curve before the threshold point, and the core memristor produces a nonlinear voltage jump at V_{th} point.

The I_M–V_M curve of the core memristor layer has a nonlinear jump in the hysteresis region, as shown in the brown curves in Fig. **6(h)–(i)**. The $\frac{dV_M}{dI_M}$ of the memristor in the NDR region happens to be equal to the opposite number of the $\frac{dV}{dI}$ value of the nonlinear R_S in this region, which is also the reason for the lateral bending of voltage on the combined I_T–V_T curve. Take nonlinear R_S with E_a = 0.16 eV as an example, $I_S > I_M$ in the low current as shown in Fig. **7(c)**. Although the I_S–V_S curve is still a smooth nonlinear line, the I_S has jump behavior in the I_S–t curve (Fig. **7(c)**). We analyze the slope of I_M–V_M curve in the NDR region, and find that the slope change from $-\left(\frac{1}{R_S}\right)_{V_{th}}$ at point D to $-\left(\frac{1}{R_S}\right)_{V_h}$ at point D'. In Fig. **7(b)**, the $R_S = \left(\frac{dV}{dI}\right)_{S,V_{th}}$ at point D is 0.13 kΩ, and the $R_S = \left(\frac{dV}{dI}\right)_{S,V_h}$ at point D' is 0.35 kΩ.

III. DUAL-CORE MEMRISTOR COMBINATION CHARACTERISTICS

In addition to the above linear and nonlinear R_S, the S-NDR type memristor can also be used to construct a nonlinear R_S. Li et al.[13] have studied this core–shell memristor model and obtained some combined I_T–V_T curves. In actual situations, due to the non-uniformity of the device or the randomness of soft breakdown during the electroforming process, multiple conductive filaments may be formed in the device.[30] Therefore, the simplest dual or triple memristor core model can be constructed for combined I_T–V_T characteristic study. Figure **8(a)** shows the schematic diagram of **dual core memristors–shell resistor (dual–cM–sR)** structure, in which the two red cylindrical areas in the inner layer represent the core memristors R_{M1} and R_{M2}, and the yellow area wrapped in the outer layer represents the shell resistance R_S. Moreover, we ignore the thermal exchange between the three areas, then the **cM–sR** structure can be simplified to the parallel structure shown in Fig **8(b)**, namely R_{M1}, R_{M2}, and large resistance R_S in parallel. For the convenience of research, the following research assumes that the R_S is infinite, the structure can be simplified as **dual core memristors (dual–cM)** structure, which also means no current passes through the shell region when conducting a CS mode of this device.

Assuming that the characteristic parameters of the I–V curves of the two core memristors are different, a combined NDR behavior can be generated. By changing the characteristic parameters of two memristors, a variety of combined I_T–V_T curve of NDR behaviors can be generated. Table **II** lists nine of the simplest possible combinations. The combined I_T–V_T curves of **S-SB1 type, S-SB2 type and double S type** have been realized in the simulation. Detail discussion will be shown as the following.

TABLE II. Nine simplest combined NDR curves. Note: Bold is the combination realized on the simulation.

Combination curve type	Snap-back 1 type	Snap-back 2 type	S type NDR
Snap-back 1 type	Double SB1 type	SB1-SB2 type	SB1-S type
Snap-back 2 type	SB2-SB1 type	Double SB2 type	SB2-S type
S type NDR	**S-SB1 type**	**S-SB2 type**	**Double S type**

3.1 Three typical combined I_T–V_T characteristics

Since R_{M1} and R_{M2} represent different regions of the same oxide film, their electrical conductivity is subject to the P–F conduction mechanism, and both exhibit S-NDR characteristics when Newton's cooling law is satisfied (see Table S2 in the supplementary material). The current mainly passes through the two core regions in the **dual–cM** structure, so the combined I_T–V_T curve is determined by the relative values of the dynamic resistances of R_{M1} and R_{M2} when the current passes. When exploring the dual-core combination characteristics, we fix the I–V characteristics of memristor 1, different combination behaviors can be achieved by changing the I–V curve characteristics of memristor 2.

Assuming that the characteristic parameters of the I–V curves of R_{M1} and R_{M2} are complete same (Fig. **9(a)**), the combined I_T–V_T curve also exhibits S-NDR characteristics (Fig. **9(e)**). The characteristic points of I–V curve of R_{M1} is the threshold point (V_{th1} = 1.173 V, I_{th1} = 0.600 mA) and hold point (V_{h1} = 1.070 V, I_{h1} = 4.293 mA). The critical resistance R_C is about 28.1 Ω, and the R_{NDR} is about 60.9 Ω which is taken from the $\frac{dV}{dI} - V$ curve as shown in Figure **10(a)**. The results of relative parameters are summarized in Table **II**. The combined I_T–V_T curve has the same voltages of V_{th} and V_h and has twice currents of I_{th} and I_h comparing with those of individual R_{M1} or R_{M2}. This is not surprise that the I_{M1}–V_{M1} curve is completely same with the I_{M2}–V_{M2} curve (Fig. **9(i)**).

TABLE II. The parameters in the table correspond to the S-NDR curve in Fig. **9(a)-9(d)** before combination.

Resistance pre-factor	Core Memristor	V_{th} (V)	I_{th} (mA)	V_h (V)	I_h (mA)	R_C (Ω)	R_{NDR} (Ω)
R_0 = 65 Ω	R_{M1} or R_{M2}	1.173	0.600	1.070	4.29	28.1	60.9
R_0 = 66 Ω	R_{M2}	1.179	0.600	1.076	4.29	27.7	60.8

R_0 = 84 Ω	R_{M2}	1.269	0.601	1.185	3.43	29.7	58.0
R_0 = 164 Ω	R_{M2}	1.556	6.35	1.529	1.93	20.8	34.2

Let's see what's happen when the characteristic parameters of the I–V curves of R_{M2} are different from those of R_{M1}. In simulation, we lightly modify the parameters of P–F model to obtain the different S-NDR characteristics. An interesting observation is obtained when the CS mode is performed on this parallel combination. The combined I_T–V_T curves show the the coexistence of the S-NDR and the SB-NDR, even we just change one parameter a little bit.

For example, we fix the parameters of R_{M1}, and change the resistance pre-factor R_0 from 65 to 66 Ω in the parameters of R_{M2}. The I–V curves of R_{M1} and R_{M2} in CS mode have little bit different in the low resistance state (Fig. **9(b)**). The combined I_T–V_T curve exhibits S-SB2 coexistence type NDR characteristics (Fig. **9(f)**). The S-NDR occurs in low current region and the SB-NDR occurs in high current region, which is typical results observed in Kumar's nanoscale devices.[2]

In Fig. **9(f)**, the second SB-NDR region, point M to which the voltage jump returns appears in the positive resistance area. The M (0.973 V, 4.16 mA) is located above the hold point (V_{h2} = 0.963 V, I_{h2} = 3.47 mA), this is the S-SB2 NDR phenomenon. The I_{M1}–V_{M1} curve has tiny loop in the high current region, while I_{M1}–V_{M1} curve has big hysteresis in the NDR region (Fig. **9(j)**), which are different from I–V curves of R_{M2} and R_{M1}.

When we fixed the parameters of R_{M1}, and change the R_0 from 65 to 84 Ω in the parameters of R_{M2}. The I–V curves of R_{M1} and R_{M2} have large different (Fig. **9(c)**), the combined I_T–V_T curve still exhibits S-SB1 coexistence type NDR characteristics (Fig. **9(g)**). In Fig. **9(g)**, the second SB-NDR region, point M to which the voltage jump returns appears in the negative resistance area. The N (0.973 V, 4.16 mA) is located below the hold point (V_{h2} = 0.963 V, I_{h2} = 3.47 mA), this is the S-SB1 NDR phenomenon. The I_{M1}–V_{M1} curve exhibits S-NDR properties, which is also different from the hysteresis I_{M2}–V_{M2} curve (Fig. **9(k)**).

When we fixed the parameters of R_{M1}, and change the R_0 from 65 to 164 Ω in the parameters of R_{M2}. The I–V curves of R_{M1} and R_{M2} have large different (Fig. **9(d)**), the combined I_T–V_T curve exhibits double S-NDR characteristics (Fig. **9(h)**). The I_{M1}–V_{M1} curve exhibits S-NDR properties, which is same with the I_{M2}–V_{M2} curve (Fig. **9(i)**).

3.2 Analysis of typical I_T–V_T characteristics

As seen from the Figs. **9(f)–9(h)**, and the first NDR region of the synthesized I_T–V_T curve is very similar to the I–V curve of R_{M1} (Figs. **9(b)–9(d)**). It is understandable since the first NDR region in the combined I_T–V_T curve is a combination of the NDR curve of R_{M1} and a nonlinear resistance of R_{M2}. Similar with the discussion in Fig. **6(d)**, we should compare the R_{NDR} of R_{M1} and $\frac{dV}{dI}$ of R_{M2} at V_{th} of R_{M1}. The VS mode on the R_{M1} and R_{M2} was performed, as shown in Figs **10(b)**. At V_{th} of R_{M1}, the corresponding differential resistance $\left(\frac{dV}{dI}\right)_{M_2@V_{th1}}$ of the core R_{M2} is shown in Figs **10(c)** as 91 Ω, 870 Ω, and 4.28 kΩ. All these values are larger than the R_{NDR} of R_{M1} (= 60.9 Ω), hence the first NDR shows the smooth S-NDR behavior (Figs. **9(f)–9(h)**).

For the second NDR region, the combined I_T–V_T curve is the combination of the NDR curve of R_{M2} and a nonlinear low resistance of R_{M1}. We should compare the R_{NDR} of R_{M2} and $\frac{dV}{dI}$ of R_{M1} at V_{th} of R_{M2}. For the R_{M2} with R_0 = 66 Ω, the V_{th} is 1.179 V. As shown in Figs **10(d)**, the corresponding $\left(\frac{dV}{dI}\right)_{M_1@V_{th2}}$ is 31 Ω, which is less than the R_{NDR} of R_{M2} (= 60.8 Ω). Hence the second NDR shows the SB-NDR behavior (Fig. **9(f)**). For SB1 or SB2 type, we should compare the R_C of R_{M2} and $\frac{dV}{dI}$ of R_{M1} at V_h of R_{M2}. For the R_{M2} with R_0 = 66 Ω, the V_h is 1.076 V. As shown in Figs **10(d)**, the corresponding $\left(\frac{dV}{dI}\right)_{M_1@V_{h2}}$ is 11 Ω, which is less than the R_C of R_{M2} (= 27.7 Ω). Hence the second NDR shows the SB2-NDR behavior (Fig. **9(f)**), where the point M is located above the hold point.

For the R_{M2} with R_0 = 84 Ω, the V_{th} is 1.269 V. The corresponding$\left(\frac{dV}{dI}\right)_{M_1@V_{th2}}$ is 38 Ω, which is less than the R_{NDR} of R_{M2} (= 58.0 Ω). Hence the second NDR shows the SB-NDR behavior (Fig. **9(g)**). For the R_{M2} with R_0 = 84 Ω, the V_h is 1.185 V. The corresponding $\left(\frac{dV}{dI}\right)_{M_1@V_{h2}}$ is 32 Ω, which is larger than the R_C of R_{M2} (= 29.7 Ω). Hence the second NDR shows the SB1-NDR behavior (Fig. **9(g)**), where the point N is located below the hold point.

For the R_{M2} with R_0 = 164 Ω, the $\left(\frac{dV}{dI}\right)_{M_1@V_{th2}}$ at V_{th}=1.556 V and the $\left(\frac{dV}{dI}\right)_{M_1@V_{h2}}$ at V_h = 1.529 V are 48 Ω and 47 Ω, respectively. Both of them are larger than the R_{NDR} of R_{M2} (= 34.2 Ω). Hence the second NDR shows the smooth S-NDR behavior (Fig. **9(h)**).

Figure **11** and **12** show the two NDR region in time domain with V_T, I_T, I_{M1}, I_{M2}, R_{M1}, R_{M2}, and R_T under the **dual–cM** structure under the CS mode. For the four cases of the R_{M2} with R_0 = 65 Ω, 66 Ω, 84 Ω, and 164 Ω, all the first V_{th} are 1.173 V, but arrives the first V_{th} at the different time. At any time, the currents go through the two cores and the current I_{M1} is equal with I_{M2}, when the two cores are completely same (Fig. **11(e)**). At the initial current, the currents go through the two cores since the close dynamic resistance $\left(\frac{dV}{dI}\right)_{M1}$ and $\left(\frac{dV}{dI}\right)_{M2}$ at small voltage (Fig. **11(f)** –**11(h)**). When the voltage approaches the relative smaller threshold point V_{th1}, the current mainly go through the R_{M1}, the $\frac{dV_{M2}}{dI_{M2}}$ at the V_{th1} is larger than $\frac{dV_{M1}}{dI_{M1}}$, then the first NDR is smooth S-NDR. When the current further increases, the R_{M1} is reaches low resistance state. When the voltage approaches the relative larger threshold point V_{th2}, the current in R_{M1} decreases and the current in R_{M2} increases since the $\frac{dV_{M1}}{dI_{M1}}$ at the V_{th2} is larger than $\frac{dV_{M2}}{dI_{M2}}$.

In addition, we also fix the parameters of R_{M1}, and change the resistance pre-factor R_0 from 65 to 24 Ω in the parameters of R_{M2}. We only observed the S-SB2 NDR, which can also be analyzed in similar way (see Fig. **S4** in the supplementary material). When we fixed the parameters of R_{M1}, and change one of other parameters (such as thermal conductance Γ_{th}, activation energy E_a, thickness of the threshold switching film t_v, relative permittivity ε_r, ambient temperature T_{amb}) of R_{M2}. Similar change trend has been observed as from S-SB2 NDR, to S-SB1 NDR, to double S-NDR. Generally, S-SB NDR is observed easily in the parallel simulations, while double S-NDR is needed the accurate design. This has been confirmed in our parallel experiments.[13]

is easy to get comparing to other NDR. Double S is needed the accurate design. This also be confirmed in the parallel experiments. Using two different physics model to respectively construct the two core memristors, both the SB2-S NDR and SB1-S NDR are also obtained in simulation (see Fig. **S5** in the supplementary material). It also infers that S-SB NDR

IV. DUAL-WINDOW OSCILLATION CHARACTERISTICS OF DOUBLE S-NDR DEVICES

4.1 Oscillation simulations with double S-NDR

In the actual case for double S-NDR, V_{th1} and V_{th2} of the two threshold voltages are close. Here we modify the parameters of R_{M1} and R_{M2} (see Table **S2** in the supplementary material), and obtain combined I_T–V_T curve exhibits double S-NDR characteristics with close V_{th1} and V_{th2}, as the blue curve in Fig. **13(a)**. These two *I*–*V* characteristics of R_{M1} and R_{M2} representing the S-NDR curves of the two core memristors have large different shapes in NDR region and low resistance region, as the black and red curves in Fig. **13(a)**, but they have close V_{th} (Table III). If we change the resistance pre-factor R_0 from 47 to 40 Ω in the parameters of R_{M2}, the double S-NDR will change to S-SB NDR.

TABLE III. The parameters in the table correspond to the S-shaped curve before combination in Fig. **13(a)**.

Combination curve type	Device	V_{th} (V)	I_{th} (mA)	V_h (V)	I_h (mA)	R_C (Ω)	R_{NDR} (Ω)
	Memristor 1	1.028	0.282	0.916	2.13	60.6	131
Double S type	Memristor 2	1.035	0.858	0.962	4.98	17.7	35
S-SB type	Memristor 2	0.983	1.010	0.900	5.60	18.06	34

Connect two core memristor devices in parallel to the oscillation circuit of Fig. **13(b)**, where the load resistance R_L = 2 kΩ and the effective capacitance C_1 = 10 nF, where the effective capacitance includes the circuit parasitic capacitance and the intrinsic capacitance of the device. In the simulation process, the two memristors and parallel capacitors are regarded as a whole device, then the current through R_L is the current through the device.

Figure **13(c)** is the simulation result of the oscillation waveform of the current passing through the device with time. As the pulse voltage continues to increase from 2.8 V to 20 V, the device waveform has experienced the process as: no oscillation (2.8 V)–oscillation (3 V, 5 V)–no oscillation (7 V, 10 V)–oscillation (16 V, 18 V)–non-oscillation (20 V), i.e. double window oscillation process. In the same time, the device shows only single window (see Fig. **S3** in the supplementary material).

The boundary of the oscillation window can be calculated by $V_{S,\,min} = V_{th} + R_L I_{th}$ and $V_{S,\,max} = V_h + R_L I_h$, as reported before. For I_T–V_T curve in Fig. **13(a)**, the threshold and hold points in first NDR region are (V_{th1} = 1.028 V, I_{th1} = 0.904 mA) and (V_{h1} = 0.916 V, I_{h1} = 2.36 mA), respectively; the threshold and hold points in first NDR region are (V_{th2} = 1.035 V, I_{th2} = 6.25 mA) and (V_{h2} = 0.962 V, I_{h2} = 8.92 mA), respectively. Using $V_{S,\,min} = V_{th} + R_L I_{th}$ and $V_{S,\,max} = V_h + R_L I_h$,[8,31] the boundaries of the oscillation window are calculated. Figure **14(a)** is the double oscillation windows in V_S – R_L plot for the double S-NDR curve.

Figure **14(b)** shows the relationship between the oscillation frequency and pulse voltage with three load resistance of 2 kΩ, 4 kΩ, and 8 kΩ. For a fixed R_L, the oscillation frequency increases with the applied voltage, and the voltage window range increases with R_L increasing. For example, for R_L = 2 kΩ, the oscillation window has two adjustable voltage ranges, and there is a non-oscillation zone between the two adjustable voltage ranges. The two adjustable voltage ranges are 2.7 V (from 2.9 V To 5.6 V) and 4.9 V (from 13.6 V to 18.5 V). For R_L = 4 kΩ, the adjustable range is increased to 5.6 V (from 4.6 V to 10.2 V) and 9.9 V (from 26.2 V to 36.1 V). The voltage ranges of the non-oscillation region corresponding to the R_L of 2 kΩ and 4 kΩ are 8 V and 16 V, respectively. For R_L =8 kΩ, the two adjustable range is increased to 11.78 V and 20.2 V, respectively, and the voltage range in the non-oscillation region is 31.2 V. The voltage range of the non-oscillation zone increases with the increase of the R_L. Each time the R_L doubles, the range of the non-oscillation zone doubles. This prediction of double window oscillation related with double S-NDR has been confirmed in actual experiments. In the following we'll give a preliminarily experimental result of a single device with double S-NDR.

4.2 Dual-window oscillation Experiments

In actual measurement, the double smooth S-NDR curve can be obtained by selecting two suitable I-V characteristic devices in parallel, which has been verified by the Li et al.[13] At the same time, for a single NDR device, a dual S-NDR characteristic curve was observed. Figure **15(a)** is the measurement result of a single Ti/NbO_x/Pt structure device in the experiment. The detail fabricated process of the device has been reported in our previous report.[8] The red *I–V* curve is the result of the CS mode, where the curve has two NDR regions. However, the black *I–V* curve measured under VS mode shows only a hysteresis and no more details. The device is connected in series with a 1 kΩ resistor for oscillation measurement, and it is found that this device also shows a double oscillation window, as shown in Fig. **15(b)**. When the input voltage is lower than 1.2 V, no oscillation is observed. When the input voltage is 1.5 V and 1.7 V, the oscillation waveform is observed, and the output frequency increases with the increase of the input voltage, as shown in Fig. **15(c)**. When the input voltage is increased to 2.0 V, although oscillation occurs, it decays quickly until it disappears. However, when the input voltage further increases to 2.2 V, the oscillation reappears. The oscillation still exists until the voltage increases to 3.0 V, and the output frequency further increases with the increase of the input voltage, as shown in Figure **15(c)**. When the input voltage is increased to 3.2 V, although oscillation occurs, it decays quickly until it disappears. The appearance-disappearance-reappearance-disappearance process of this oscillation can be repeated well in the experiment, which is qualitatively consistent with the double-window oscillation predicted by the above simulation. Of course, in the actual measurement, not all double S-NDR can have double windows, and there is a great correlation with the parasitic capacitance/device capacitance. There is also heat capacity, and further simulation and experiments are still in progress.

V. CONCLUSION

In this work, the NbO_x memristor device is regarded as a **cM–sR** structure, assuming that the current distribution in the film is uneven and highly localized, considering the effect of the current distribution in the film on the equivalent circuit of the device. When the R_S is linear resistance, the load line analysis method gives the conditions that the R_S should meet when generating SB-NDR and S-NDR curves, and analyzes the relationship between the size of the hysteresis area and the R_S. When the R_S is a non-linear resistance, the $\frac{dV}{dI}$ value of the non-linear shell corresponding to the V_{th} of the *I–V* curve of the core memristor layer is the characteristic point that determines the behavior of the NDR region.

When two core memristors layer are connected in the **dual–cM** structure, nine possible simple combinations are proposed, and the combined *I–V* characteristics are analyzed by borrowing the conclusion when the R_S is a non-linear resistance, and the customized NDR characteristics of combined NbO_x memristor in the device can be realized. Aiming at the curve showing the dual S-NDR behavior in the combined *I–V* curve, the analysis of oscillation behavior is conducted and the phenomenon of dual window oscillation is predicted. Finally, the oscillation behavior of the dual window was confirmed by preliminary simulation and experiment.

SUPPLEMENTARY MATERIAL

See the supplementary material for the simulated parameters of the P–F model.

DATA AVAILABILITY STATEMENT

The data that support the findings of this study are available from the corresponding author upon reasonable request.

ACKNOWLEDGEMENTS

This work was partly supported by the National Natural Science Foundation of China (NNSFC; Nos. 11674241 and 11774253) and the Natural Science Foundation of Tianjin City (No. 18JCYBJC18000).

REFERENCES

[1]S. Yu, Proceedings of the IEEE **106,** 260 (2018).
[2]S. Kumar, J. P. Strachan, and R. S. Williams, Nature **548,** 318 (2017).
[3]Y. Zhou and S. Ramanathan, Proceedings of the IEEE **103,** 1289 (2015).
[4]A. A. Sharma, J. A. Bain, and J. A. Weldon, Exploratory Solid-State Computational Devices and Circuits, IEEE Journal on **1,** 58 (2015).

[5]G. A. Gibson, S. Musunuru, J. Zhang, K. Vandenberghe, J. Lee, C.-C. Hsieh, W. Jackson, Y. Jeon, D. Henze, and Z. Li, Applied Physics Letters **108,** 023505 (2016).
[6]A. Alexandrov, A. Bratkovsky, B. Bridle, S. Savel'Ev, D. Strukov, and R. Stanley Williams, Applied Physics Letters **99,** 202104 (2011).
[7]S. Slesazeck, H. Mähne, H. Wylezich, A. Wachowiak, J. Radhakrishnan, A. Ascoli, R. Tetzlaff, and T. Mikolajick, RSC Advances **5,** 102318 (2015).
[8]X. Liu, S. Li, S. K. Nandi, D. K. Venkatachalam, and R. G. Elliman, Journal of Applied Physics **120,** 124102 (2016).
[9]M. D. Pickett and R. S. Williams, Nanotechnology **23,** 215202 (2012).
[10]G. A. Gibson, Advanced Functional Materials **28,** 1704175 (2018).
[11]S. Kumar, Z. Wang, N. Davila, N. Kumari, K. J. Norris, X. Huang, J. P. Strachan, D. Vine, A. L. D. Kilcoyne, Y. Nishi, and R. S. Williams, Nature Communications **8,** 658 (2017).
[12]S. Kumar and R. S. Williams, Nature Communications **9,** 2030 (2018).
[13]S. Li, X. Liu, S. K. Nandi, S. K. Nath, and R. G. Elliman, Advanced Functional Materials **29,** 1905060 (2019).
[14]S. K. Nandi, S. K. Nath, A. E. El‐Helou, S. Li, X. Liu, P. E. Raad, and R. G. Elliman, Advanced Functional Materials **29,** 1906731 (2019).
[15]S. K. Nath, S. K. Nandi, A. El-Helou, X. Liu, S. Li, T. Ratcliff, P. E. Raad, and R. G. Elliman, Physical Review Applied **13,** 064024 (2020).
[16]J. M. Goodwill, G. Ramer, D. Li, B. D. Hoskins, G. Pavlidis, J. J. McClelland, A. Centrone, J. A. Bain, and M. Skowronski, Nature Communications **10,** 1 (2019).
[17]M. Herzig, M. Weiher, A. Ascoli, R. Tetzlaff, T. Mikolajick, and S. Slesazeck, Journal of Physics D: Applied Physics **52,** 325104 (2019).
[18]S. R. Ovshinsky, Physical Review Letters **21,** 1450 (1968).
[19]J. Sakai, Journal of Applied Physics **103,** 103708 (2008).
[20]Y. W. Lee, B.-J. Kim, J.-W. Lim, S. J. Yun, S. Choi, B.-G. Chae, G. Kim, and H.-T. Kim, Applied Physics Letters **92,** 162903 (2008).
[21]D. Li, J. M. Goodwill, J. A. Bain, and M. Skowronski, Nanoscale **9,** 14139 (2017).
[22]J. M. Goodwill, A. A. Sharma, D. Li, J. A. Bain, and M. Skowronski, ACS applied materials & interfaces **9,** 11704 (2017).
[23]J. M. Goodwill, D. K. Gala, J. A. Bain, and M. Skowronski, Journal of Applied Physics **123,** 115105 (2018).
[24]M. Noman, A. A. Sharma, Y. Meng Lu, R. Kamaladasa, M. Skowronski, P. A. Salvador, and J. A. Bain, Applied Physics Letters **104,** 113510 (2014).
[25]K. Jung, Y. Kim, W. Jung, H. Im, B. Park, J. Hong, J. Lee, J. Park, and J.-K. Lee, Applied Physics Letters **97,** 233509 (2010).
[26]S. M. Bohaichuk, M. Muñoz Rojo, G. Pitner, C. J. McClellan, F. Lian, J. Li, J. Jeong, M. G. Samant, S. S. Parkin, and H.-S. P. Wong, ACS Nano **13,** 11070 (2019).
[27]S. K. Nath, S. K. Nandi, S. Li, and R. G. Elliman, Applied Physics Letters **114,** 062901 (2019).
[28]N. Shukla, A. Parihar, E. Freeman, H. Paik, G. Stone, V. Narayanan, H. Wen, Z. Cai, V. Gopalan, and R. Engel-Herbert, Scientific reports **4,** 4964 (2014).
[29]A. Ascoli, S. Slesazeck, H. Mahne, R. Tetzlaff, and T. Mikolajick, IEEE Transactions on Circuits and Systems I: Regular Papers **62,** 1165 (2015).
[30]H. Clarke, L. Deremo, J. Anderson, S. Ganguli, and P. J. Shamberger, Nanotechnology **31,** 075706 (2020).
[31]P. Zhang, S. Li, Y. Bo, and X. Liu, Journal of Applied Physics **126,** 125112 (2019).

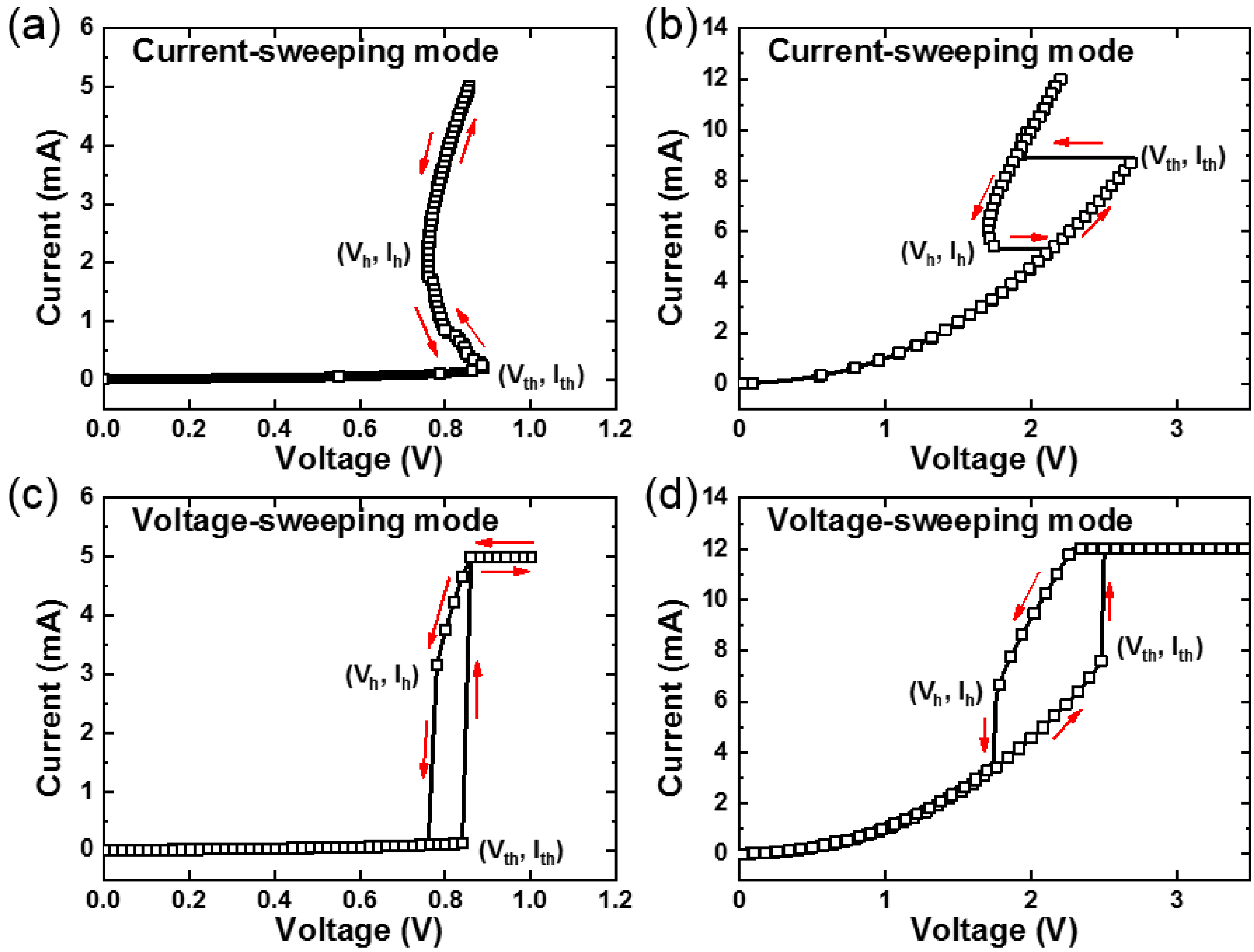

FIG. 1. Measured *I*–*V* characteristics of NbO_x devices under CS operation mode showing (a) continuous S-NDR and (b) discontinuous SB-NDR behavior, respectively. Under VS operation mode, both (c) S-NDR and (d) SB-NDR show threshold switching behavior with hysteresis curves.

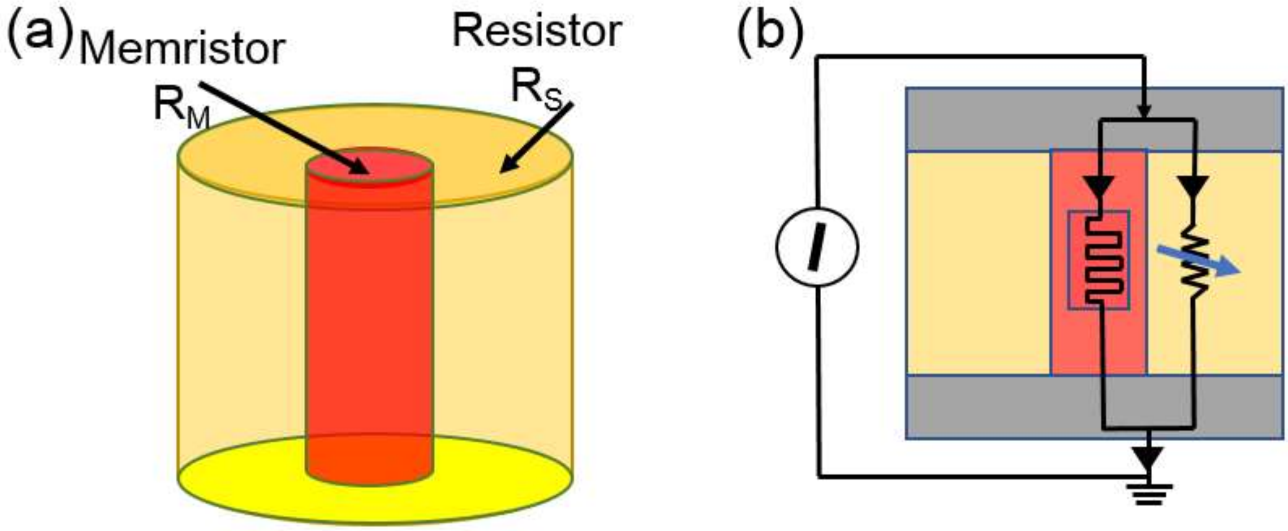

FIG. 2. (a) Core memristor–shell resistor (cM–sR) structure model diagram. (b) Equivalent circuit diagram of NbO_x device under CS mode, without considering thermal exchange between the core and shell.

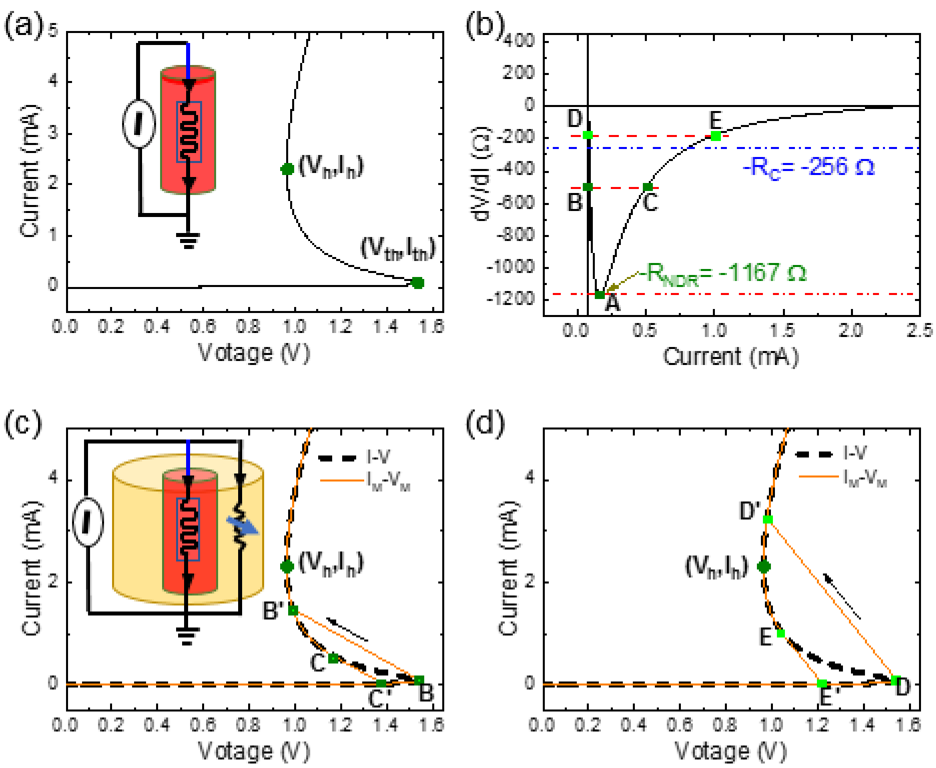

FIG. 3. (a) The inherent *I*–*V* curve of the independent core memristor under CS mode. The inset shows the schematic diagram of a three-dimensional two-terminal core-only memristor, which could be obtain in scaling down experiments. (b) The relationship between differential resistance ($\frac{dV}{dI}$) and current for core-only memristor. The red dashed lines correspond to the $\frac{dV}{dI}$ of -180 Ω and -500 Ω, respectively. The comparison between the hysteresis I_M–V_M curve (black solid line) of the core memristor and the inherent *I*–*V* curve of the independent core memristor (red dashed line) with the shell resistance of (c) 500 Ω and (d) 180 Ω. The inset shows the schematic diagram of a three-dimensional two-terminal cM–sR under CS mode.

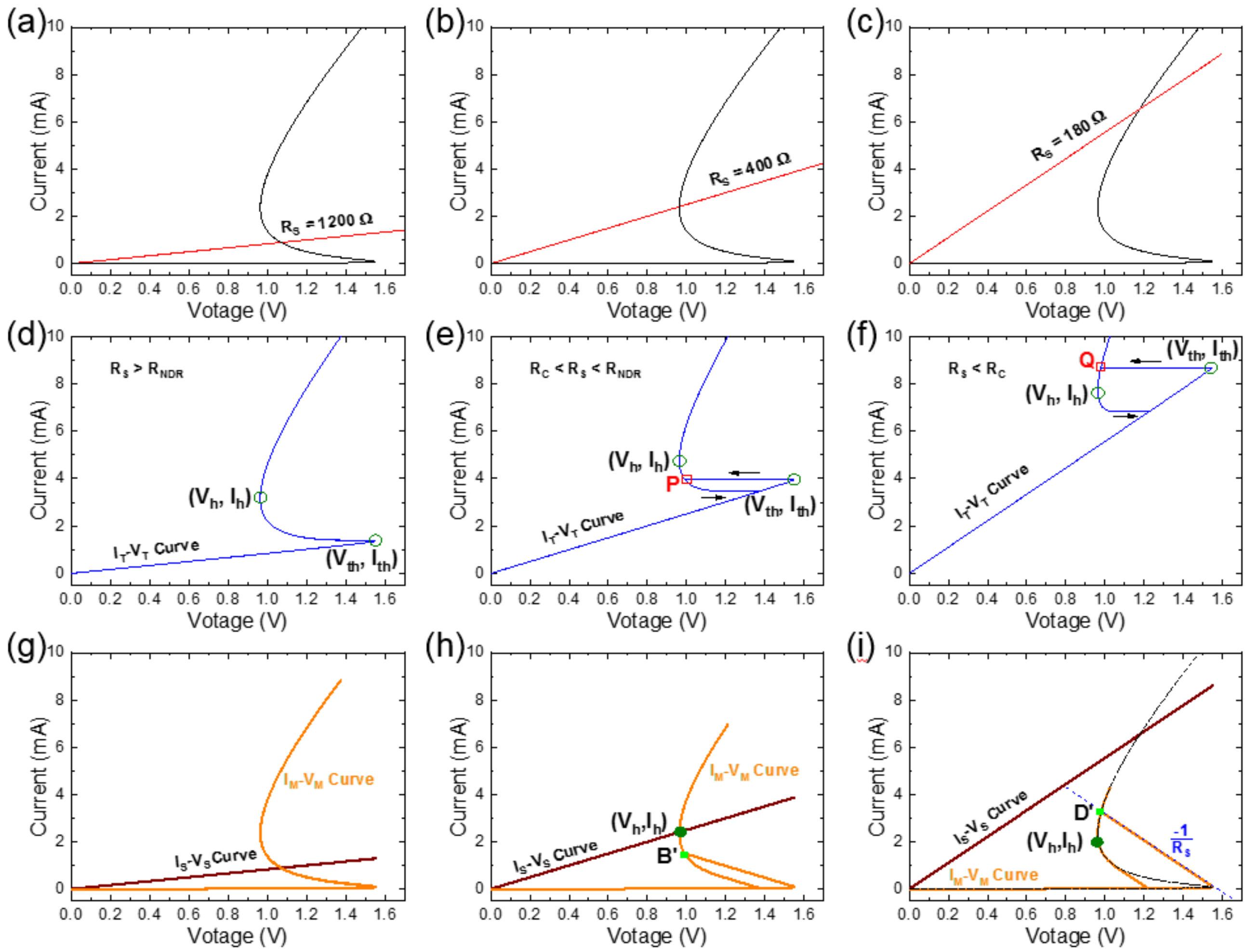

FIG. 4. The inherent *I*–*V* curves of the independent core memristor (red line) and shell resistor (black curve) with the shell resistance of (a) 1200 Ω, (b) 400 Ω, and (c) 180 Ω under CS mode. (d) When R_S = 1200 Ω > R_{NDR}, the combined I_T–V_T curve (blue curve) of cM–sR structure under CS mode shows smooth S-NDR characteristic without hysteresis. (e) When R_C < R_S = 400 Ω < R_{NDR}, the combined (blue curve) shows SB1-NDR characteristic with hysteresis and the hysteresis zone only appears in the I_T–V_T curve NDR region. (f) When R_S = 180 Ω < R_C, the combined I_T–V_T curve (blue curve) shows SB2-NDR characteristic with hysteresis and the hysteresis zone appears in the low positive resistance region. (g)–(i) The I_M–V_M and the I_S–V_S curves in measuring states of cM–sR structure model with different combinations.

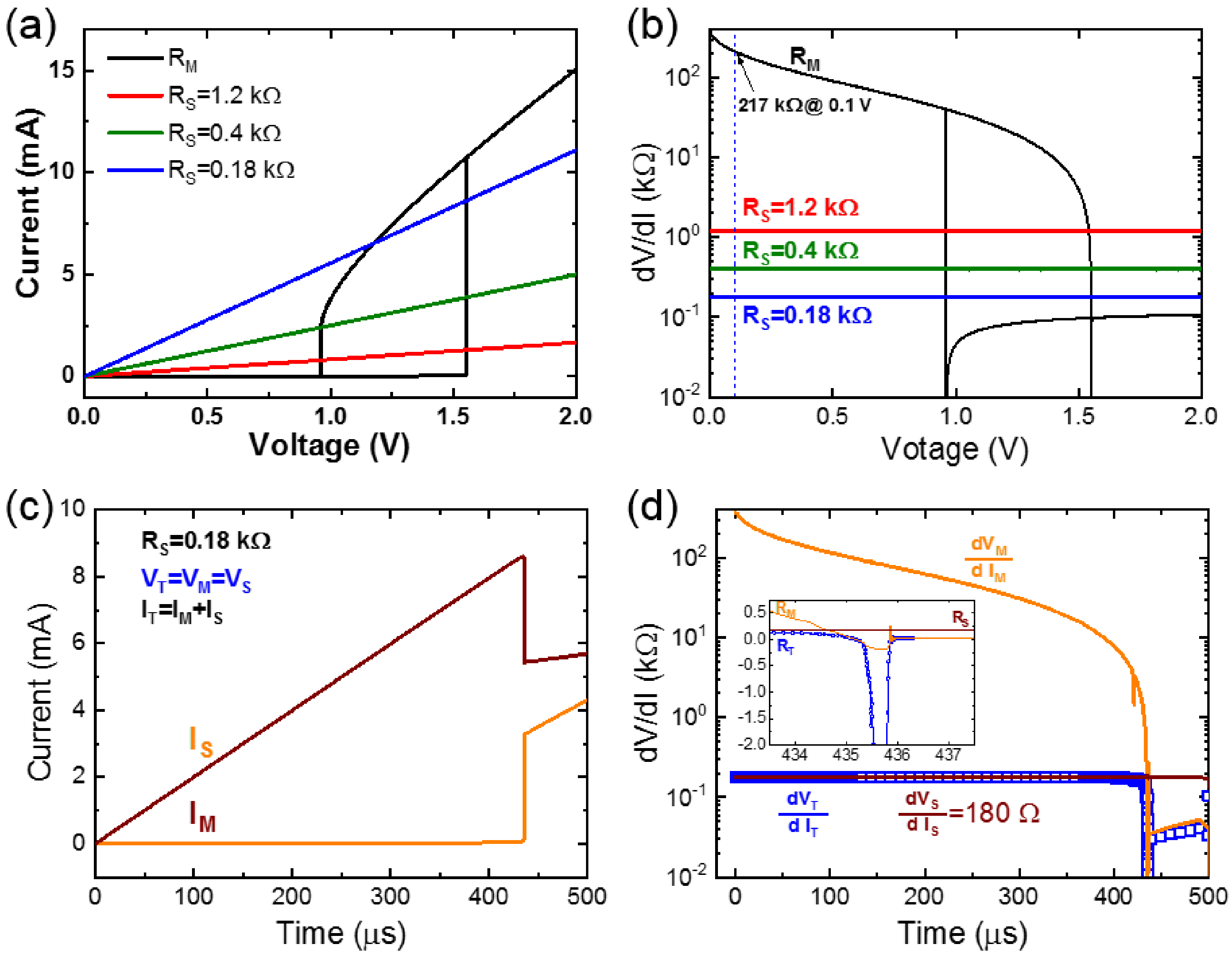

FIG. 5. (a) The inherent *I*–*V* curves and (b) the corresponding $\frac{dV}{dI}$–*V* curves of the independent core memristor and shell resistor with different R_S under VS mode. (c) The currents I_M and I_S under CS mode flowing through the R_M and R_S. (d) The dynamic resistance of $\frac{dV_M}{dI_M}$, $\frac{dV_S}{dI_S}$, and $\frac{dV_T}{dI_T}$ in the simulation case of R_S = 180 Ω.

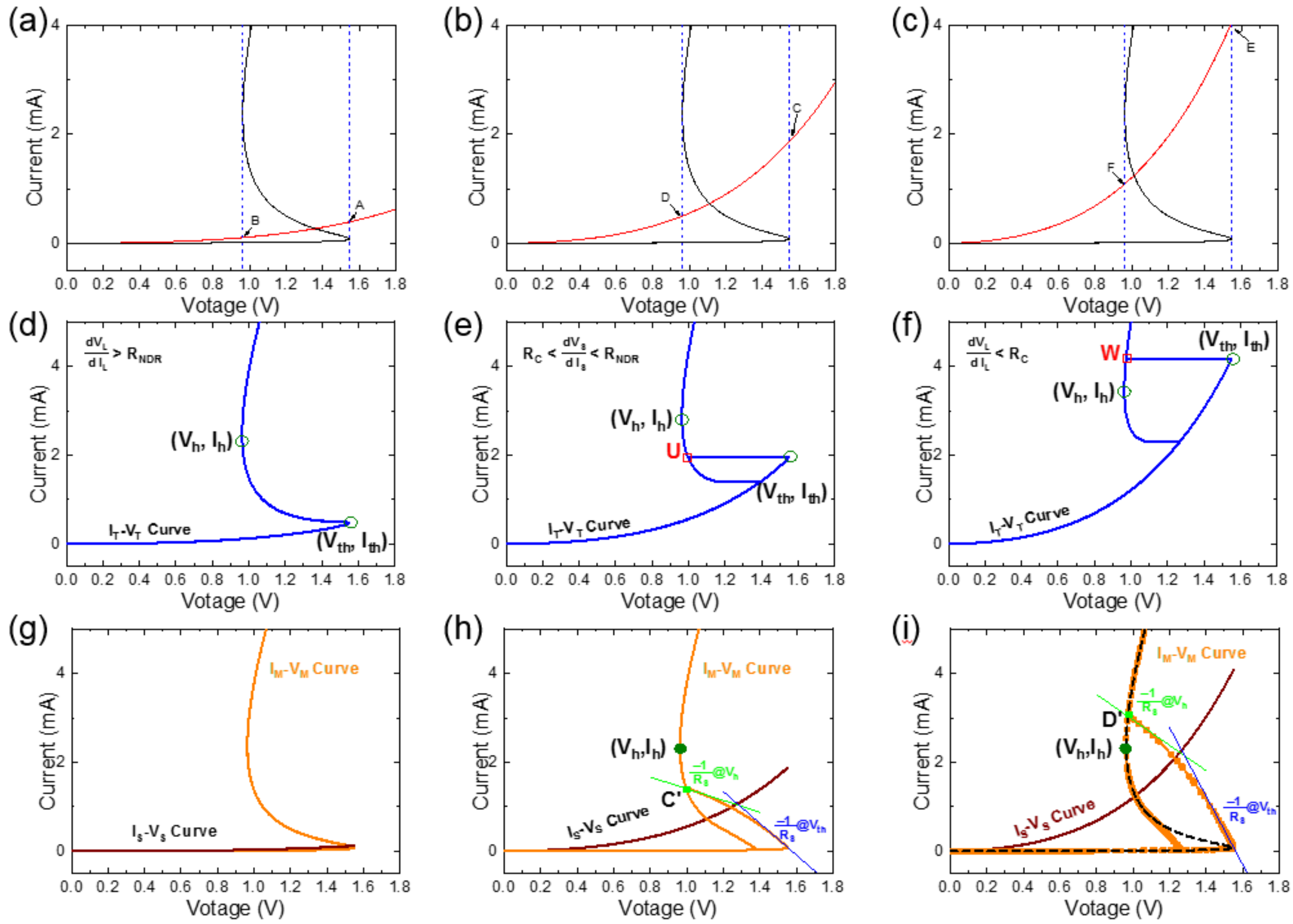

FIG. 6. The inherent *I*–*V* curves of the independent core memristor (red line) and nonlinear shell resistor (black curve) with (a) E_a = 0.22 eV, (b) E_a = 0.18 eV, and (c) E_a = 0.16 eV under CS mode. (d) When E_a = 0.22 eV, the combined I_T–V_T curve (blue curve) of cM–sR structure under CS mode shows smooth S-NDR characteristic without hysteresis. (e) When E_a = 0.18 eV, the combined I_T–V_T curve (blue curve) shows SB1-NDR characteristic with hysteresis and the hysteresis zone only appears in the NDR region. (f) When E_a = 0.16 eV, the combined I_T–V_T curve (blue curve) shows SB2-NDR characteristic with hysteresis and the hysteresis zone appears in the low positive resistance region. (g)–(i) The I_M–V_M and the I_S–V_S curves in measuring states of cM–sR structure model with different combinations.

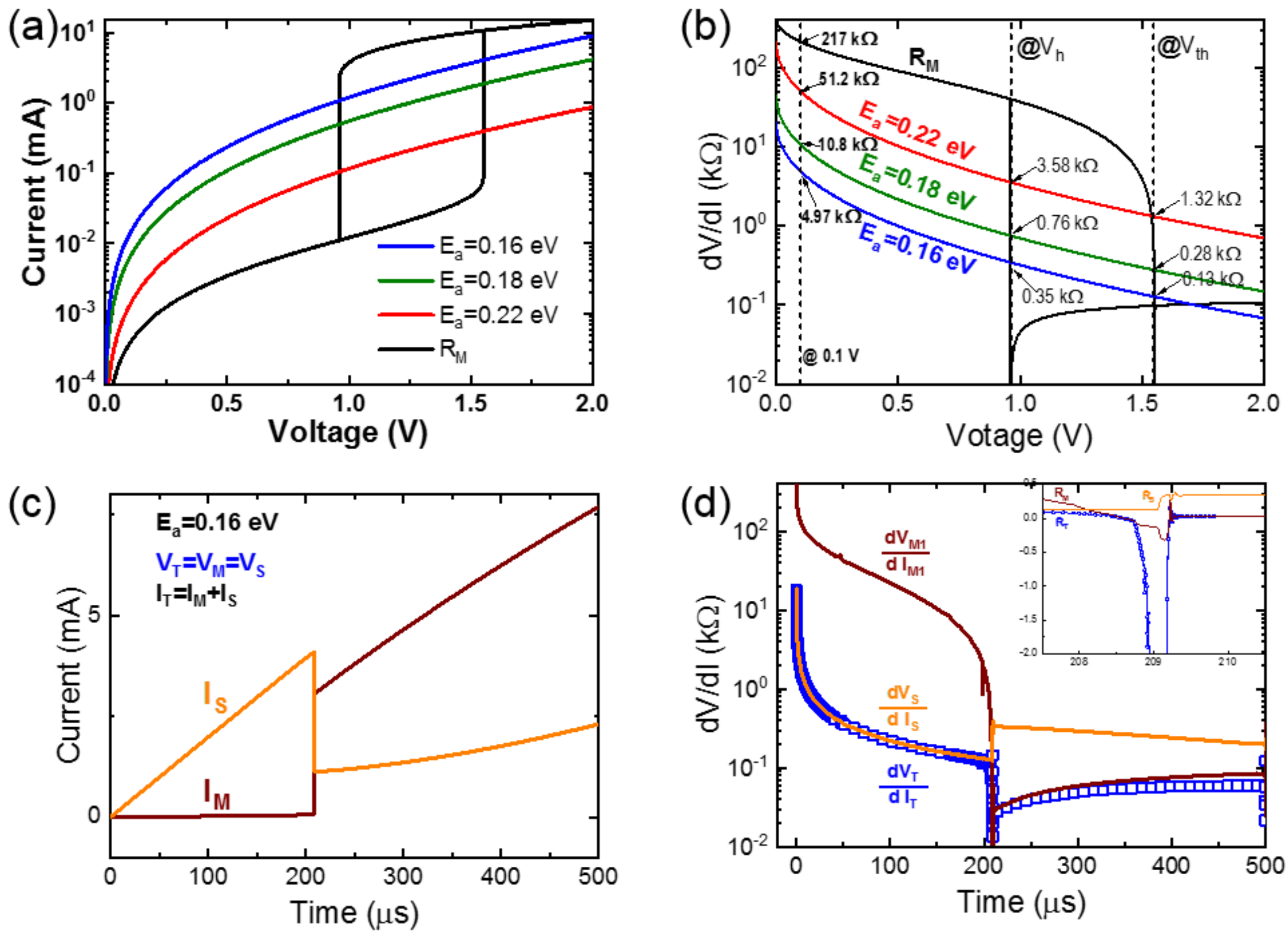

FIG. 7. (a) The inherent *I*–*V* curves and (b) the corresponding $\frac{dV}{dI}$–*V* curves of the independent core memristor and nonlinear shell resistor with different R_S under VS mode. (c) The currents I_M and I_S under CS mode flowing through the R_M and R_S. (d) The dynamic resistance of $\frac{dV_M}{dI_M}$, $\frac{dV_S}{dI_S}$, and $\frac{dV_T}{dI_T}$ in the simulation case of R_S = 180 Ω.

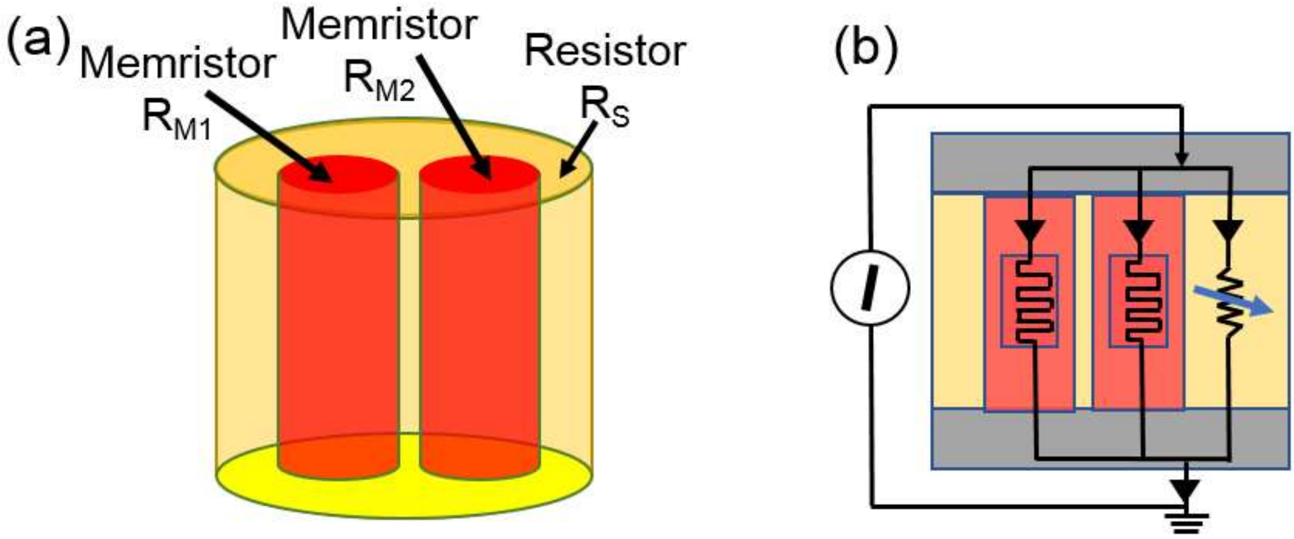

FIG. 8. (a) Dual-core memristor (cM–sR) structure model diagram. (b) Equivalent circuit diagram of device with dual conducting filaments under CS mode, without considering thermal exchange between the core and shell.

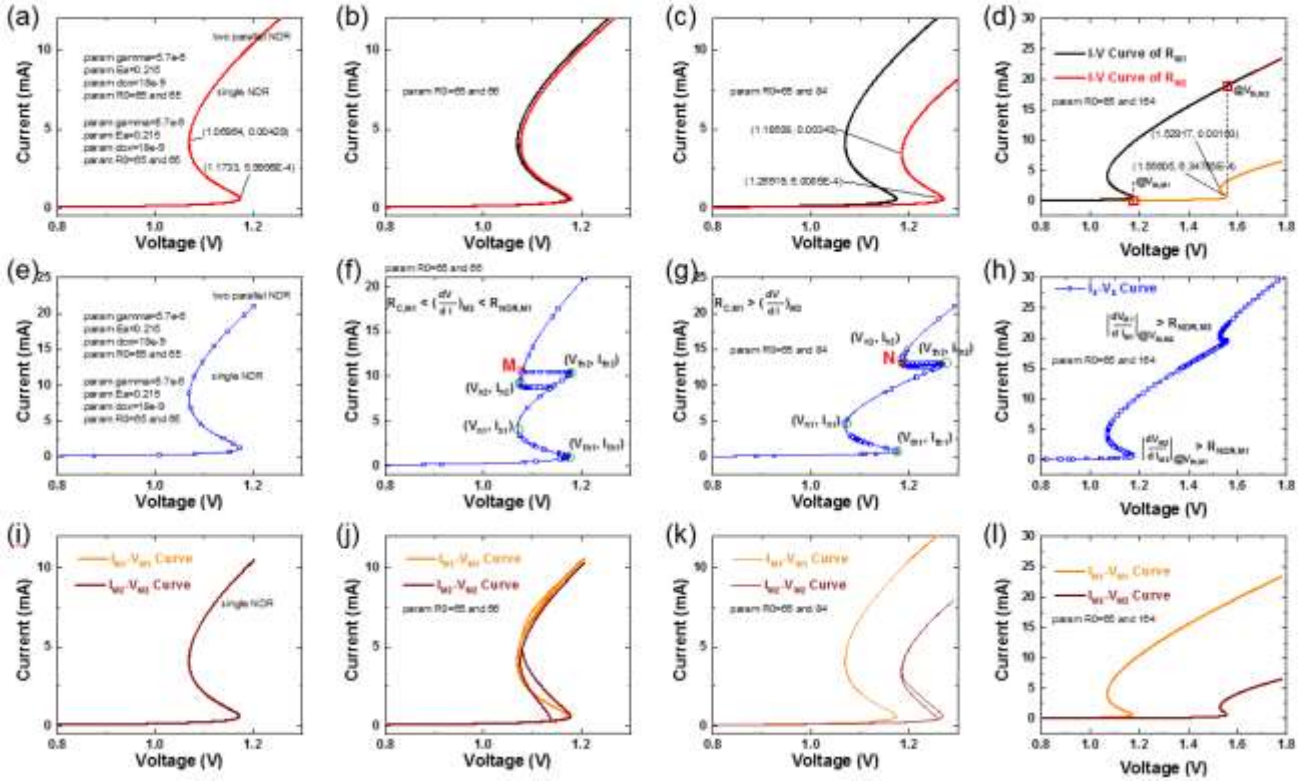

FIG. 9. (a)–(d) The inherent *I*–*V* curves of the two-independent core memristor in four R_{M1} (black curve) and R_{M2} (red curve) combination under CS mode. The parameters of R_{M1} are fixed and the resistance pre-factor R_0 in the parameters of R_{M2} is change from 65 to 164 Ω. (e) When R_{M1} (R_0 = 65 Ω) and R_{M2} (R_0 = 65 Ω) are completely same, the combined I_T–V_T curve (blue curve) of cM–sR structure under CS mode shows smooth S-NDR characteristic without hysteresis. (f) When R_{M1} (R_0 = 65 Ω) and R_{M2} (R_0 = 66 Ω) are different, the combined I_T–V_T curve (blue curve) shows S-SB2 NDR characteristic. (g) When R_{M1} (R_0 = 65 Ω) and R_{M2} (R_0 = 84 Ω) are different, the combined I_T–V_T curve (blue curve) shows S-SB1 NDR characteristic. (h) When R_{M1} (R_0 = 65 Ω) and R_{M2} (R_0 = 164 Ω) are different, the combined I_T–V_T curve (blue curve) shows double S-NDR characteristic. (i)–(l) The I_M–V_M and the I_S–V_S curves in measuring states of cM–sR structure model with different combinations.

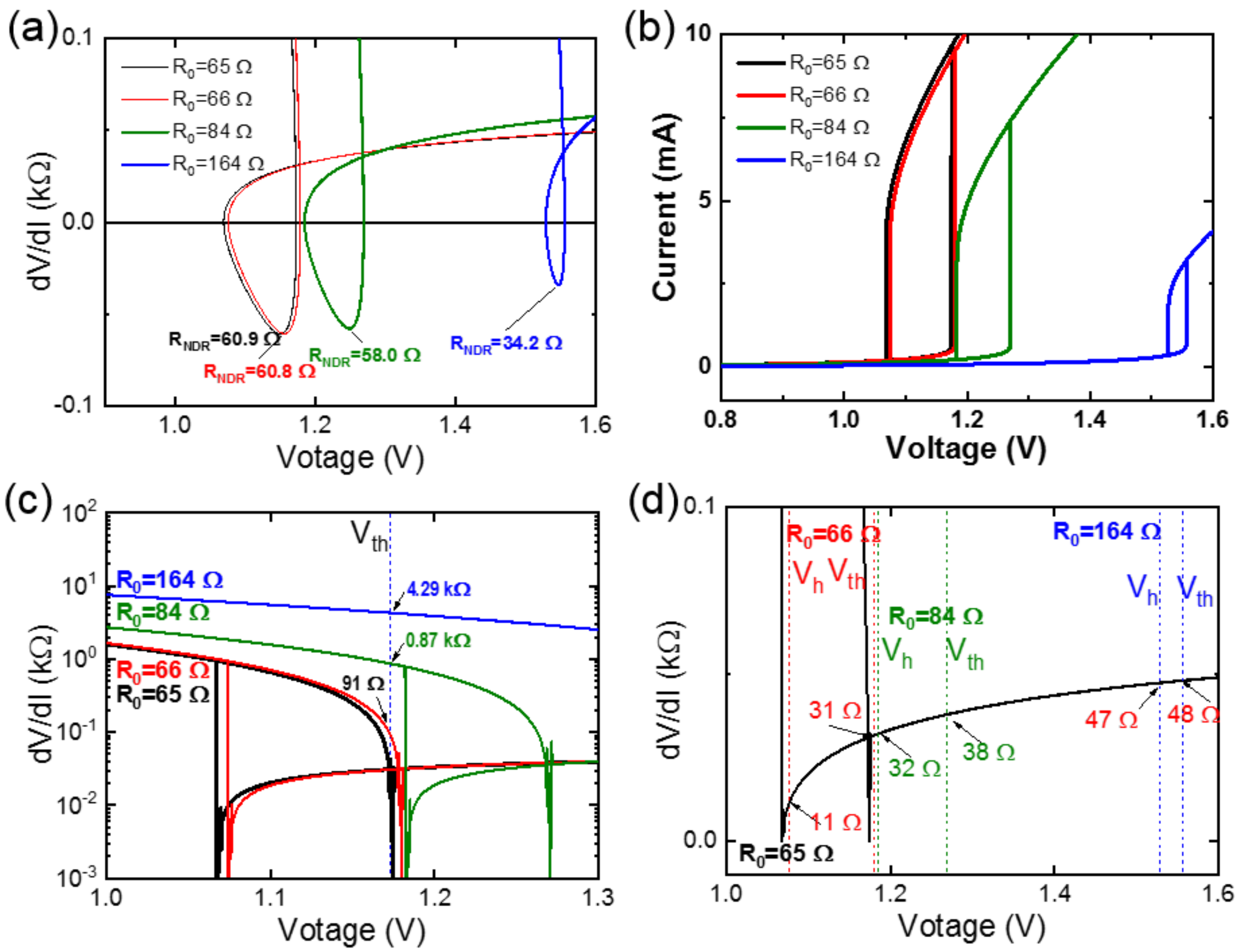

FIG. 10. (a) The relation between the differential resistance $\left(\frac{dV}{dI}\right)_M$ of the independent core memristor and total voltage in the CS mode to define their values of R_{NDR}. (b) The inherent I–V curves and (c) the corresponding $\frac{dV}{dI}$–V curves of the independent core memristor under the VS mode to define their values of $\left(\frac{dV}{dI}\right)_{M2}$ at V_{th} of the R_{M1}. (d) The $\frac{dV}{dI}$–V curves of the R_{M1} under the VS mode to define the values of $\left(\frac{dV}{dI}\right)_{M1}$ at V_{th} and V_h of the R_{M2}.

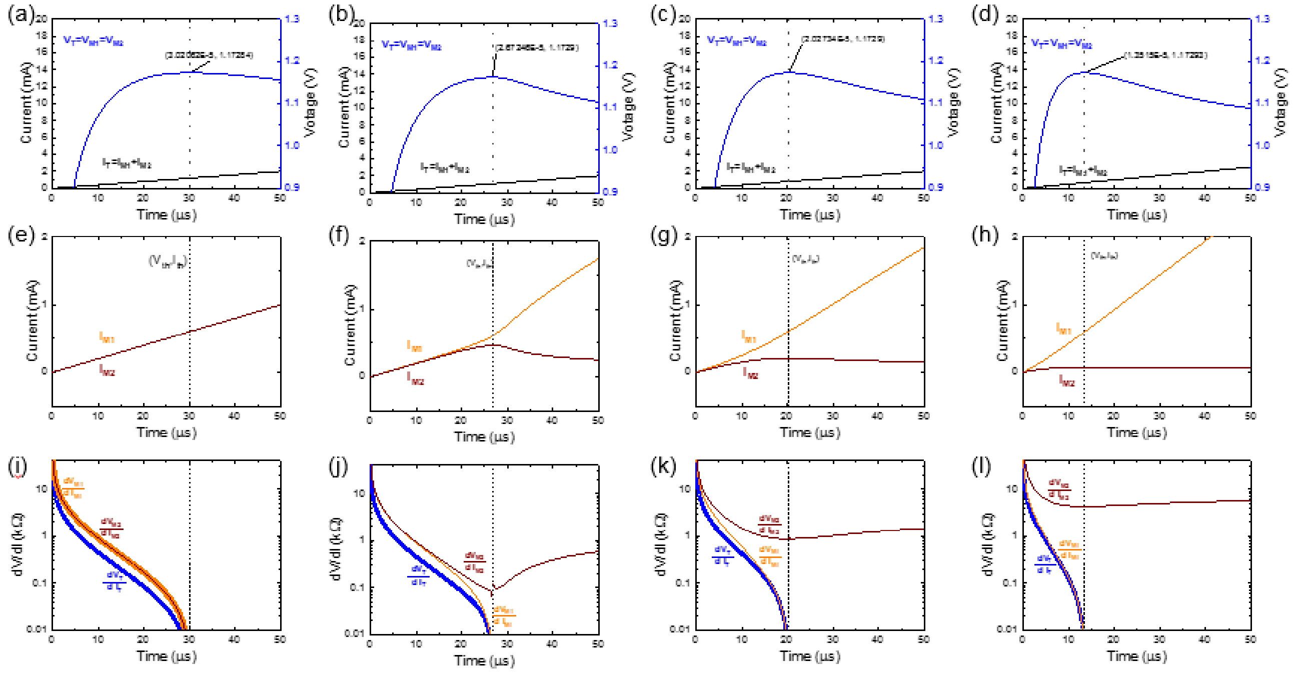

FIG. 11. The change behaviors of different circuit parameters in the time domain of first NDR (0-50 μs) for four R_{M1} and R_{M2} combination under the CS mode. (a)–(d) The total voltage V_T and total current I_T. (e)–(h) The currents I_M and I_S flowing through the R_M and R_S. (i)–(l) The dynamic resistance of $\frac{dV_{M1}}{dI_{M1}}$, $\frac{dV_{M2}}{dI_{M2}}$, and $\frac{dV_T}{dI_T}$.

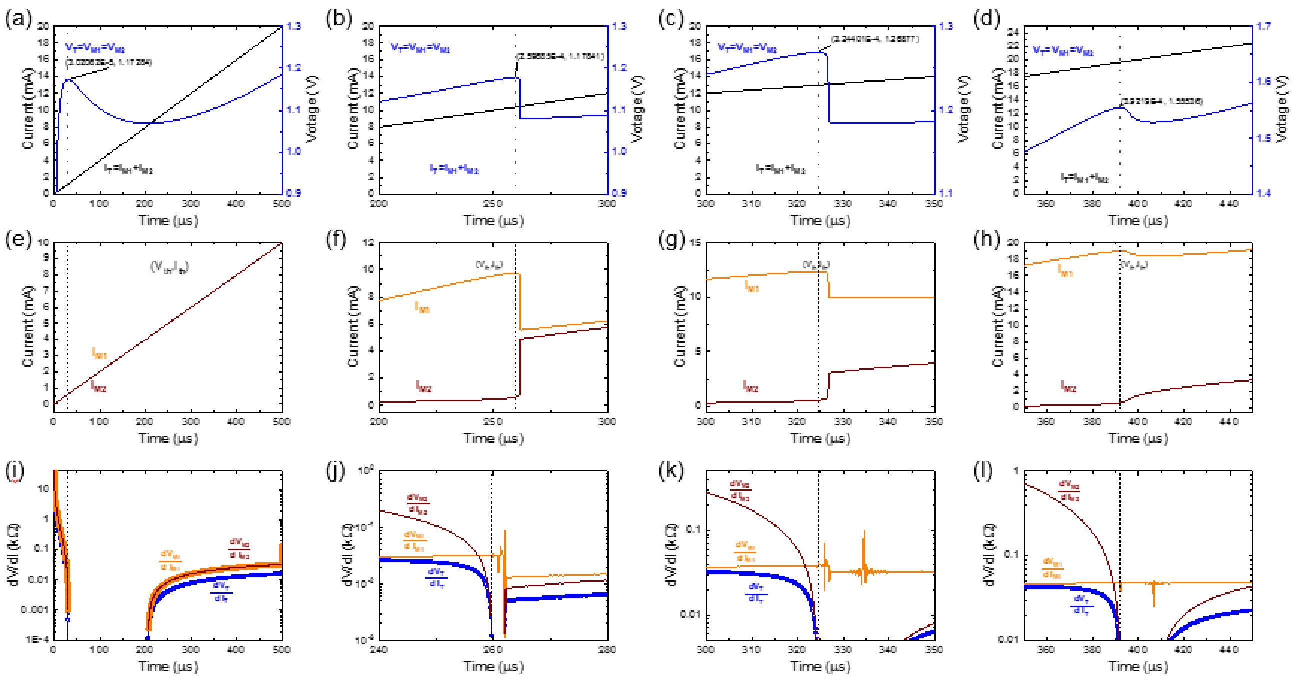

FIG. 12. The change behaviors of different circuit parameters in the time domain of second NDR (after 200 μs) for four R_{M1} and R_{M2} combination under the CS mode. (a)–(d) The total voltage V_T and total current I_T. (e)–(h) The currents I_M and I_S flowing through the R_M and R_S. (i)–(l) The dynamic resistance of $\frac{dV_{M1}}{dI_{M1}}$, $\frac{dV_{M2}}{dI_{M2}}$, and $\frac{dV_T}{dI_T}$.

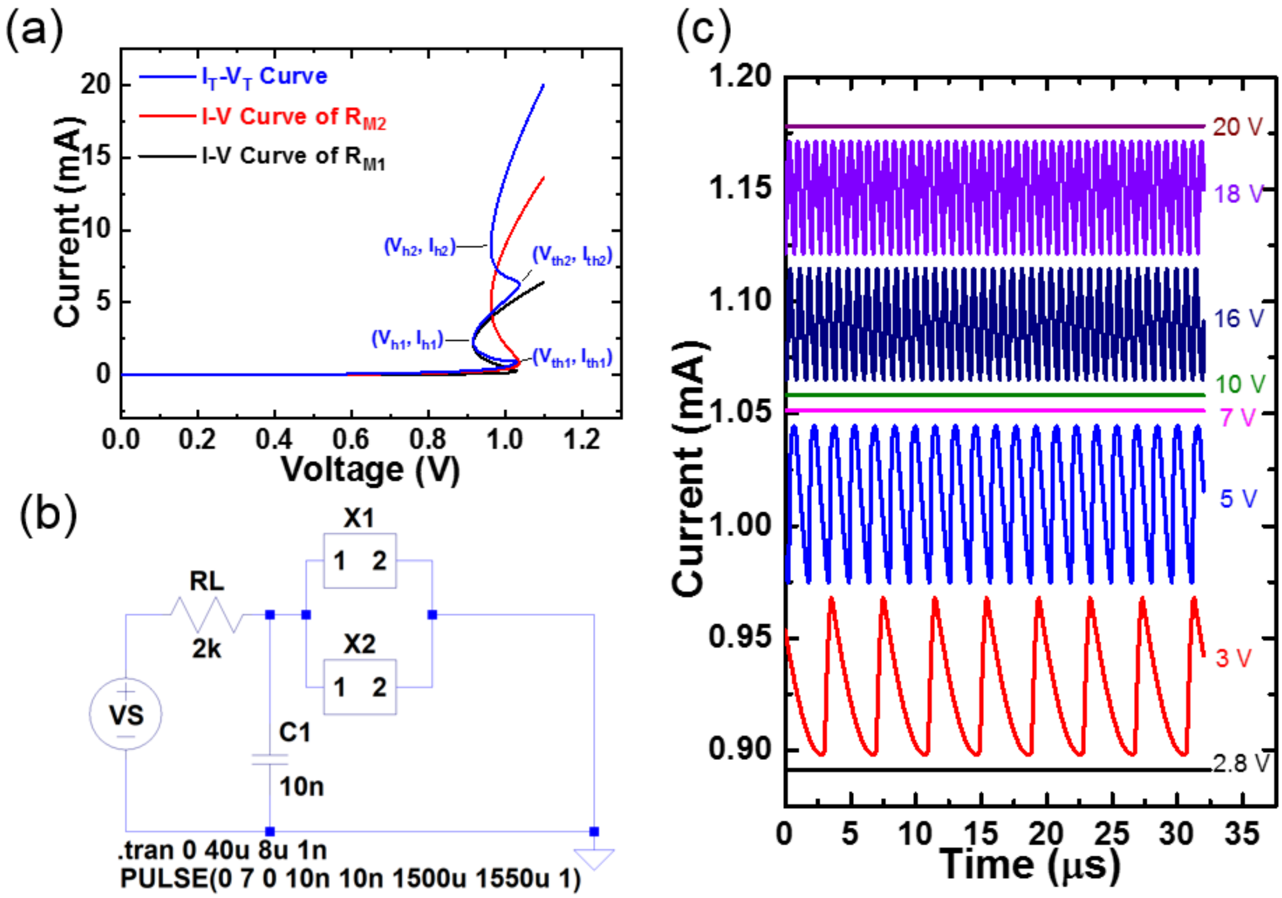

FIG. 13. (a) The combined I_T–V_T curve is a double S-NDR curve with close V_{th1} and V_{th2}. (b) The oscillation circuit diagram containing the double S-NDR device. (c) When $R_L = 2$ kΩ, the time domain waveform diagram under different pulse voltages, where the voltage range is 2.8 V–20 V.

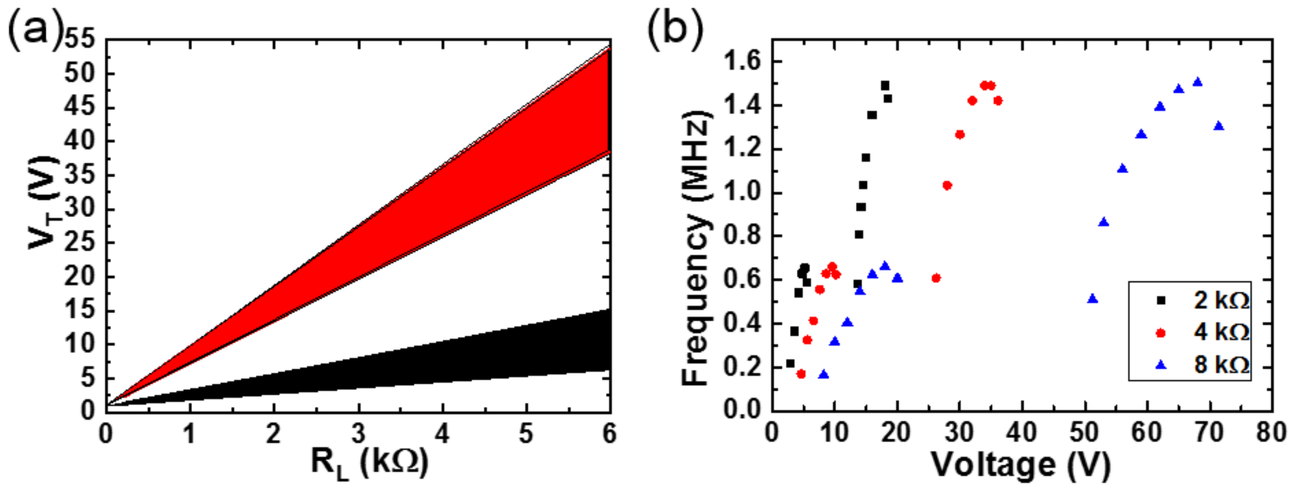

FIG. 14. (a) The dual oscillation windows in V_T–R_L diagram corresponding to dual S-NDR device. (b) The relationship between the oscillation frequency and the pulse voltage amplitude under different load resistances (black square R_L = 2 kΩ, red triangle R_L = 4 kΩ, blue triangle R_L = 8 kΩ).

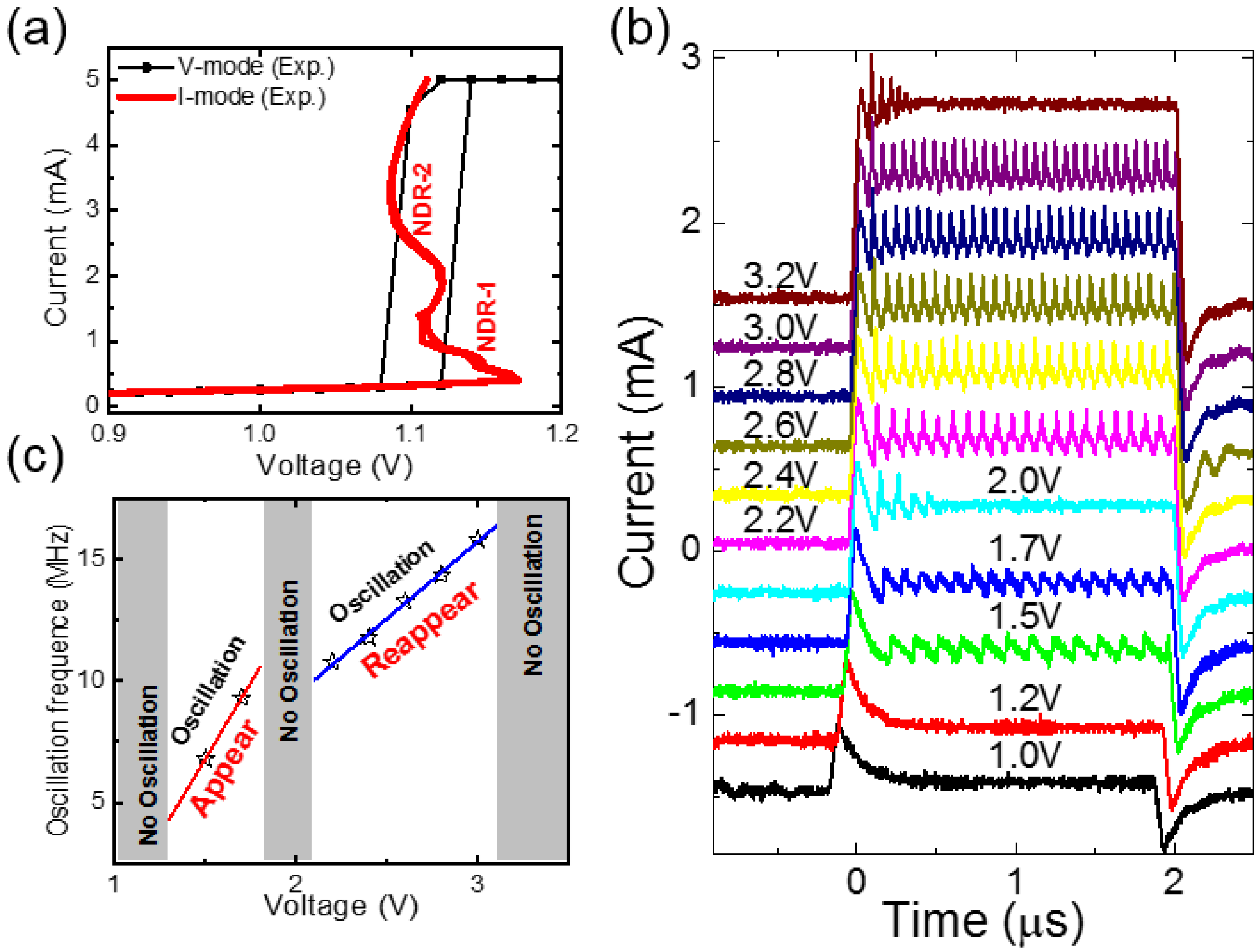

FIG. 15. (a) Experimentally measured *I*–*V* curve of NbO_x device with CS mode (red curve) and VS mode (black curve). (b) Experimentally measured oscillation waveform of double S-NDR device with the voltage in range of 1 V–3.2 V. (c) The relation between the oscillation frequency and the pulse voltage amplitude with load resistance R_L = 1 kΩ.

Supplementary Material

Understanding composite negative differential resistance in niobium oxide memristors

Xinjun Liu, Peng Zhang, Shimul Kanti Nath, Shuai Li, Sanjoy Kumar Nandi, and Robert Glen Elliman

1) Parameters for circuits and memristor model used in the simulation

Poole-Frenkel (P-F) emission is a thermally activated conduction mechanism, due to the electrons emitted from the trap into the dielectric conduction band under the action of the electric field, When an electric field is applied to the insulator, the reduction of the field-induced barrier increases the possibility of electron emission. Slesazeck et al. **[R1]** gave the P-F model of micron-level volatile memristors in Nb_2O_5:

$$R_m = R_0 e^{\frac{1}{kT_m}\left(E_a - q\sqrt{\frac{qE}{\pi\varepsilon_0\varepsilon_r}}\right)} \tag{S1}$$

Equation (S1) gives the dependence of device resistance R_m and temperature T_m according to the P-F formula, where k is the Boltzmann constant, E_a is the activation energy, q is the electron charge, and ε_r is the conductive filament inside the Nb_2O_5 film R_0 is the relative dielectric constant, R_0 is the fitting parameter.

$$\frac{dT_m}{dt} = \frac{R_m i_m^2 - \Gamma_{th}\Delta T}{C_{th}} \tag{S2}$$

The equation of state (1-7) is Newton's law of cooling, which represents the dynamic change of the internal temperature of the conductive filament with time. The first term on the right represents the Joule heating term, the second term represents the heat dissipation term, and C_{th} represents the heat capacity, Γ_{th} Stands for thermal conductivity.

Equations (1-6) and (1-7) and Ohm's law $v_m = i_m R_m$ together describe the volatile memristor model. They compared the simulation results of the model with the experimental data and achieved a good consistency, indicating that it is reasonable to use the memristor model to explain the negative differential resistance characteristics of NbO_x materials.

Table S1: Memristor parameters used in simulation for the Poole-Frenkel conduction model. [R1].

Model Parameters (Unit)	Symbol	Values for Figs. 3, 4, 5	Values for Figs. 7	Values for Figs. 8, 9
Thermal conductance ($W \cdot K^{-1}$)	Γ_{th}	1.7×10^{-6}	5.7×10^{-6}	2.4×10^{-6} for R_{M1} and 6.7×10^{-6} for R_{M2}
Activation Energy (eV)	E_a	0.21 eV for R_M; 0.22 eV, 0.18 eV, and 0.16 eV for R_S with nonlinear shell resistor	0.215	0.202 for R_{M1} and 0.204 for R_{M2}
Thickness of the threshold switching volume (nm)	t_v	88	18	23 for R_{M1} and 19 for R_{M2}
Resistance prefactor (Ω)	R_0	120	65 for R_{M1} and 65, 66, 84, 164 for R_{M1}	110 for R_{M1} and 47 for R_{M2}
Thermal capacitance ($J \cdot K^{-1}$)	C_{th}	2.5×10^{-14}	2.5×10^{-14}	2.5×10^{-14}
Boltzmann constant ($J \cdot K^{-1}$)	k_B	1.38×10^{-23}	1.38×10^{-23}	1.38×10^{-23}
Elementary charge (C)	e	1.6×10^{-19}	1.6×10^{-19}	1.6×10^{-19}
Vacuum permittivity ($F \cdot m^{-1}$)	ε_0	8.85×10^{-12}	8.85×10^{-12}	8.85×10^{-12}
Relative permittivity of the threshold switching volume	ε_r	45	45	45
Ambient temperature (K)	T_{amb}	298	298	298

2) The state equations of the equivalent circuit of the **cM–sR** model in a CC mode

The parallel connection between S-NDR and constant resistance is the simplest combination in the **cM–sR** model. By combining the *I–V* curve of S-NDR core and the linear *I–V* curve, a synthetic I_T–V_T curve will be obtained. In parallel state under test, the I_M–V_M curve of the S-NDR core memristor and the I_S–V_S curve of shell resistance are different from those in their individual state. When a CC mode is applied to the equivalent circuit of the **cM–sR** model, the state equations of this circuit can be listed by Kirchhoff's law:

$$I_T = I_M + I_S = \frac{V_M}{R_M} + \frac{V_S}{R_S} \tag{S3}$$

$$V_T = V_M = V_S \tag{S4}$$

It can be obtained through transformation:

$$I_T = V_M \left(\frac{1}{R_M} + \frac{1}{R_S}\right) = V_M \left(\frac{R_M + R_S}{R_M R_S}\right) \tag{S5}$$

The voltage V_M and current I_M on the S-NDR device are further derived as:

$$V_M = I_T \left(\frac{R_M R_S}{R_M + R_S}\right) \tag{S6}$$

$$I_M = \frac{V_M}{R_M} = I_T \left(\frac{R_M R_S}{R_M + R_S}\right) \cdot \frac{1}{R_M} = \frac{I_T R_S}{R_M + R_S} \tag{S7}$$

3) Currents-voltage curves for dual-core parallelled model with fixed parameters of R_{M1} and various resistance pre-factor R_0 (from 65 to 24 Ω) in the parameters of R_{M2}

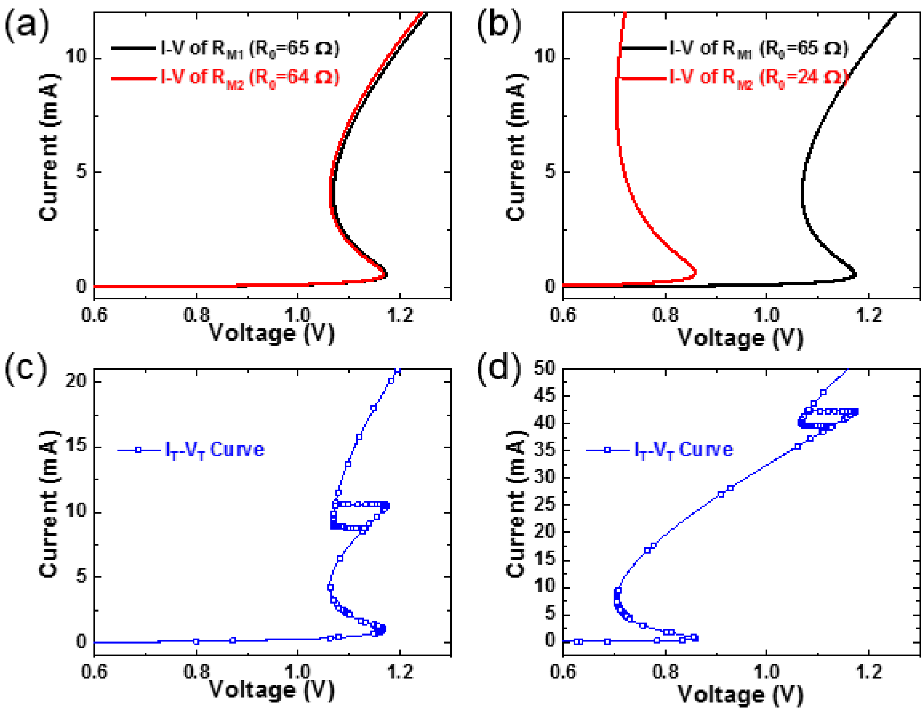

Fig. S1. (a)–(b) The inherent *I–V* curves of the dual core memristor in two combination of R_{M1} (black curve) and R_{M2} (red curve) under CC mode. (c) When R_{M1} (R_0 = 65 Ω) and R_{M2} (R_0 = 64 Ω) are lightly different, the combined I_T–V_T curve (blue curve) shows S-SB2 NDR characteristic. (d) When R_{M1} (R_0 = 65 Ω) and R_{M2} (R_0 = 24 Ω) are distinctly different, the combined I_T–V_T curve (blue curve) also shows S-SB2 NDR characteristic.

4) Oscillation simulations with S-SB2 NDR

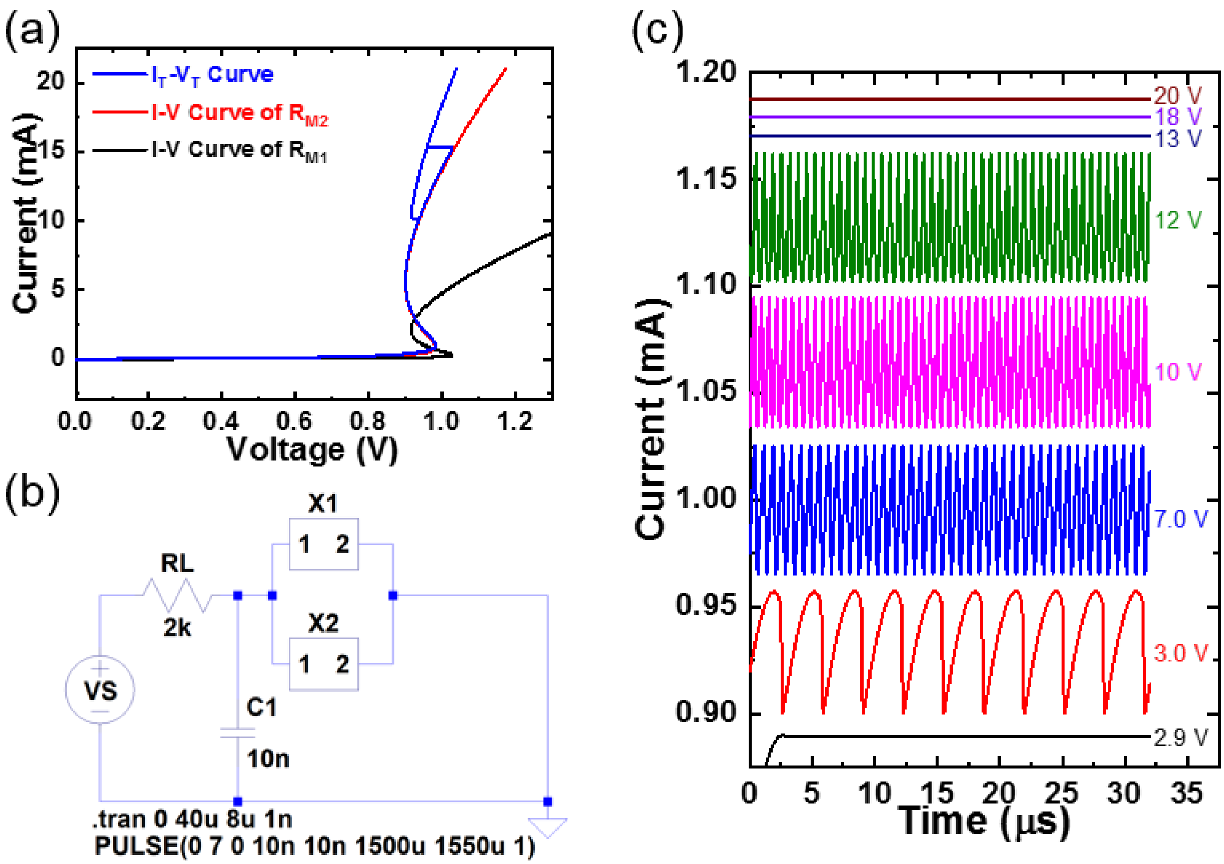

Fig. S2. (a) The combined I_T–V_T curve is a S-SB2 NDR curve with different V_{th1} and V_{th2}. (b) The oscillation circuit diagram containing the S-SB2 NDR device. (c) When R_L = 2 kΩ, the time domain waveform diagram under different pulse voltages, where a oscillation window is observed in the voltage range is 2.9 V–20 V.

References:

[R1] J. Radhakrishnan, S. Slesazeck, H. Wylezich, T. Mikolajick, A. Ascoli, and R. Tetzlaff, "A physics-based Spice model for the Nb_2O_5 threshold switching memristor." CNNA 2016; 15th International Workshop on Cellular Nanoscale Networks and their Applications. VDE, 2016.